Chemical Science

ROYAL SOCIETY OF CHEMISTRY

MINIREVIEW

View Article Online
View Journal | View Issue

Cite this: *Chem. Sci.*, 2020, **11**, 8686

All publication charges for this article have been paid for by the Royal Society of Chemistry

Designing composite solid-state electrolytes for high performance lithium ion or lithium metal batteries

Tengfei Zhang, †*[a] Wenjie He,†[a] Wei Zhang, *[b] Tao Wang, [a] Peng Li, [a] ZhengMing Sun [b] and Xuebin Yu*[c]

Received 4th June 2020
Accepted 18th July 2020

DOI: 10.1039/d0sc03121f

rsc.li/chemical-science

Solid-state electrolytes (SSEs) are capable of inhibiting the growth of lithium dendrites, demonstrating great potential in next-generation lithium-ion batteries (LIBs). However, poor room temperature ionic conductivity and the unstable interface between SSEs and the electrode block their large-scale applications in LIBs. Composite solid-state electrolytes (CSSEs) formed by mixing different ionic conductors lead to better performance than single SSEs, especially in terms of ionic conductivity and interfacial stability. Herein, we have systematically reviewed recent developments and investigations of CSSEs including inorganic composite and organic–inorganic composite materials, in order to provide a better understanding of designing CSSEs. The comparison of different types of CSSEs relative to their parental materials is deeply discussed in the context of ionic conductivity and interfacial design. Then, the proposed ion transfer pathways and models of lithium dendrite growth in composites are outlined to inspire future development of CSSEs.

Introduction

As efficient energy storage devices, batteries, including nickel-metal hydride (Ni-MH) batteries, lead-acid batteries and lithium-ion batteries (LIBs), can be effectively combined with renewable energy sources such as solar energy, wind energy and hydrogen energy, and such batteries are expected to be advanced energy storage systems and reduce fossil fuel dependence.[1] In the past few decades, the energy density of LIBs has been higher than that of many other types of batteries; they have

[a]Jiangsu Key Laboratory of Electrochemical Energy-Storage Technologies, College of Materials Science and Technology, Nanjing University of Aeronautics and Astronautics, Nanjing 210016, China. E-mail: zhangtengfei@nuaa.edu.cn

[b]Jiangsu Key Laboratory of Advanced Metallic Materials, School of Materials Science and Engineering, Southeast University, Nanjing, 211189, China. E-mail: w69zhang@seu.edu.cn

[c]Department of Materials Science, Fudan University, Shanghai 200433, China. E-mail: yuxuebin@fudan.edu.cn

† T. Z. and W. H. contributed equally to this work.

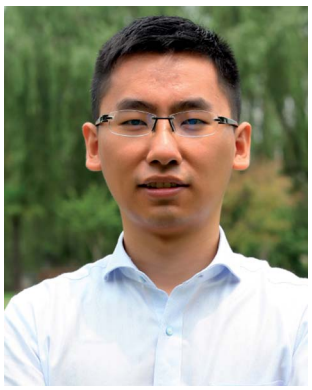

Tengfei Zhang is an associate professor in the College of Materials Science and Technology at Nanjing University of Aeronautics and Astronautics (NUAA). He obtained his BE from the School of Materials Science and Engineering, Central South University, China and PhD in Advanced Materials from Hokkaido University, Japan. He then worked as a JSPS fellow at Hokkaido University and an assistant professor at Hiroshima University. His current research interests are in the areas of solid-state electrolytes, hydrogen storage materials, and in situ TEM.

Wenjie He received his M.S. degrees in material engineering from Shaanxi University of Science and Technology in 2018. He is currently pursuing his PhD degree under the supervision of Prof. Xiaogang Zhang in applied chemistry at Nanjing University of Aeronautics and Astronautics. His current research focuses on advanced materials for electrochemical energy storage devices, such as lithium-ion batteries and all-solid-state batteries.

been widely used in the fields of personal electronics, hybrid and electrical vehicles, and grid energy conversion–storage systems.[2,3] Although LIBs have appeared in daily life in many forms, currently available commercial LIBs still cannot meet the stringent or increasing demand for high-performance equipment in modern society.[4–16] There is an urgent need to develop batteries with higher energy density and longer cycle life, along with an acceptable level of safety and an affordable price. Liquid electrolytes demonstrate high conductivity and excellent electrode surface wettability, but they often suffer from the problems of insufficient electrochemical and thermal stability, low ion selectivity and poor safety.[17–25]

Concurrently, lithium metal, as a negative electrode, exhibits low redox potential (−3.045 V) and high theoretical specific capacity (3860 mA h g^{-1}), while also being light-weight (M = 6.94 g mol^{-1}, D = 0.534 g cm^{-3}).[26,27] However, as the charging and discharging process continues, the gradual growth of lithium dendrites can pierce the separator, leading to a short circuit in the battery.[28] Furthermore, the electrolyte is a flammable substance. If leaked, it can cause serious safety accidents. In addition, an unstable solid electrolyte interphase (SEI) is formed between the liquid electrolyte and the electrode material.[27,29–35] The appearance of an SEI will reduce battery capacity and shorten the cycle life of the battery. Therefore, LIBs using lithium metal as the negative electrode have poor cycling performance and serious safety problems. The emergence of SSEs is expected to enable lithium metal to be used as a negative material in all solid-state battery systems, resulting in a higher energy density than what is currently available. Replacing liquid electrolytes with SSEs can also effectively inhibit the generation of SEI films and improve the cycle performance of batteries. At the same time, the size of the battery is reduced, and its application scope is expanded. More importantly, compared to liquid electrolytes, SSEs (*e.g.*, inorganic ceramic electrolytes) do not leak and are non-flammable, and thus, safety is greatly enhanced. The use of solid-state electrolytes instead of liquid electrolytes can not only overcome the liquid electrolyte durability problem, but also provide an important avenue for developing next-generation LIBs.

With the emergence of LIBs, research on SSEs continued. Manthiram *et al.* provided a detailed account of the development of SSEs in 2017.[11,36] Solid electrolytes can be divided into two categories: solid polymer materials and inorganic materials. Typical conductive polymers are polyethylene oxide (PEO),[37] polyacrylonitrile (PAN),[38,39] polymethyl methacrylate (PMMA),[40,41] and polyvinylidene fluoride (PVDF).[42,43] In polymer electrolytes, the polymer long chains are partially shifted above the glass transition temperature, thereby creating a binding site for ion hopping, and the constant hopping of ions in a specific direction can achieve an ion transport effect. Typical inorganic lithium-ion conductive materials include lithium phosphorus oxynitride (LiPON),[44] perovskite,[45] sodium superionic conductor (NASICON),[46–48] garnet,[15,49–56] sulfide,[10,17,57–64] halide,[65–70] and hydride based materials.[71–76] Among them, the high ionic conductivity of solid crystalline materials can be attributed to the large number of structural defects or special crystal structures. The former involves point defect-based ion diffusion mechanisms, including simple vacancy mechanisms and relatively complex diffusion mechanisms, while the latter involves usually two types of sublattices, which are composed of immobile and mobile ions. The ionic diffusion process in glass materials is similar to that of crystalline materials in that ions move between active sites.

High ionic conductivity, low ionic area specific resistance, high electronic area specific resistance, high ionic selectivity, a wide electrochemical stability window, good chemical compatibility, excellent thermal stability, excellent mechanical properties, simple fabrication processes, and environmental friendliness are the main properties of a good solid-state electrolyte.[11] Much progress has been made in improving the above-mentioned properties. Perovskite-type oxide compounds, in the form of ABO_3, show a lithium ionic conductivity as high as

Wei Zhang is an associate professor in School of Materials Science and Engineering at Southeast University. He obtained his MASc in Chemistry and PhD in Nanotechnology from the University of Waterloo. After joining Southeast University in 2016, he established the Surface Science and Bionanomaterials Laboratory, and is working on both fundamental and applied research to meet the growing need of nanotechnology in advanced materials, e.g. multifunctional and smart hydrogels and aerogels, flexible energy storage devices or electronic packaging. He was awarded the Periodic Table of Younger Chemists in 2019 by the Chinese Chemical Society.

Xuebin Yu received his PhD degree from the Shanghai Institute of Microsystem and Information Technology, Chinese Academy of Science in 2004. He then worked as a postdoctoral fellow at the University of Nottingham and the University of Wollongong from January 2005 to December 2006 and March 2007 to March 2008, respectively. In 2008, he joined Fudan University and now works as a professor in the Department of Materials. His research interests cover hydrogen storage, fuel-cell integration with hydrogen systems, hydride-based solid-state electrolytes, lithium/sodium-ion batteries, and preparation of nanomaterials for energy storage.

10^{-3} S cm^{-1} in the bulk portion, which has been attributed to the presence of a significant amount of equivalent deficient sites for lithium ions to substitute and freely move in bulk crystals. Additionally, these compounds (*e.g.*, $Li_{3x}La_{2/3x}TiO_3$) have a high grain boundary resistance that is related to the reduction of Ti^{4+} to Ti^{3+} upon contact with Li metal.[77,78] Garnet-type materials, such as $Li_5La_3Ta_2O_{12}$ and $Li_5La_3Nb_2O_{12}$, have also been considered fast lithium-ion conductors since 2003.[79] Since then, a new garnet-type ceramic of $Li_7La_3Zr_2O_{12}$ has been discovered with a high ionic conductivity (2.44×10^{-4} S cm^{-1}).[80] Although these ceramics are chemically stable with electrodes, their poor interfacial compatibility with lithium metal limits their applications in the field of solid-state batteries. Furthermore, the volume expansion and shrinkage of the electrode during the charging/discharging process will cause the electrolyte to crack and thereby lose its capacity. The mechanical flexibility of SSEs determines whether they easily crack.[81] Therefore, electrolytes should have a moderate elastic modulus. In general, the mechanical flexibility of sulfide-type materials is better than that of oxide-type materials. Additionally, the replacement of oxygen ions with sulfur ions, which have a larger radius, can not only provide more migration space for lithium ions, but also reduce bonding strength. As a result, compared with oxides, sulfides exhibit higher lithium-ion conductivity with a value of approximately 10^{-2} to 10^{-4} S cm^{-1} at room temperature (RT).[82] For example, $Li_{10}GeP_2S_{12}$ exhibits an extremely high lithium ionic conductivity of 1.2×10^{-2} S cm^{-1} at RT owing to its three-dimensional framework structure.[16] Notably, the low output and high cost of germanium limit the possibility of its large-scale production and application. Moreover, most sulfide solid electrolytes are not stable and can easily react with H_2O, releasing a highly toxic gas: H_2S.[83] More recently, a complex hydride lithium superionic conductor, $0.7Li(CB_9H_{10})$–$0.3Li(CB_{11}H_{12})$, has been developed with excellent stability against lithium metal and a high conductivity of 6.7×10^{-3} S cm^{-1} at 298 K.[84] However, the compatibility of the above material with cathode materials is poor due to the reducibility of complex hydrides. Unlike brittle crystalline solid inorganic electrolytes (SIEs), solid polymer electrolytes (SPEs) are highly flexible. Nonetheless, SPEs have not been applied in commercial batteries due to their low ionic conductivities (10^{-6} to 10^{-8} S cm^{-1}) at RT and poor electrochemical stability (<4 V).[85]

Based on the excellent work of many researchers in analyzing various electrolytes, it is difficult for a single type of SSE to fully satisfy the challenging requirements mentioned above. This has led to a growing research interest in CSSEs, which aims to develop promising SSEs by combining the advantages and eliminating the drawbacks of both inorganic and organic solid electrolytes. A brief overview of CSSEs is first introduced (Fig. 1).[11] Inspired by the radar plot from the work of Manthiram *et al.*[11] (Fig. 1a), it is necessary to summarize the recent progress of composite solid-state electrolytes. Herein, this review systematically surveys recent CSSE progress, with special emphasis on the following aspects: polymer-based, oxide-based, hydride-based, sulfide-based, and halide-based SSEs. The conductivity, interphase behavior, electrochemical stability and properties of these electrolytes, along with their associated all-solid-state LIBs are also systematically summarized and characterized (Fig. 1b). We focus on the design of the electrolyte itself and discuss the challenges in developing these materials. Additionally, CSSEs are discussed with regard to their application in many Li battery systems, including Li-ion, Li-metal, and Li–sulfur batteries.

Progress of CSSEs

Solid-state ionics is the science of ion transport in solids. The term "ionic" has been used for ionic conduction since the early days of electrochemical research, but mainly for liquid electrolytes. The field of solid-state ionics first started with the work of Faraday in heated solid electrolytes of Ag_2S and PbF_2 in 1833.[86] In general, the mobility of ions in solids is very slow, and hardly contributes to electrical conductivity. However, high ionic mobility is observed in certain types of inorganic ceramics, organic polymers, and composite materials, and their ionic conductivities are comparable to that of a liquid. In the 1960s, a ceramic-based β-alumina ($Na_2O \cdot 11Al_2O_3$) was found to possess a remarkable sodium-ion transport characteristic, and was successfully used in a high-temperature sodium–sulfur (Na–S) battery for grid energy conversion–storage systems.[87] It is marked as a milestone and subsequently boosted the increase in practical applications of SSEs. For example, improved Na–S battery modules were developed and made commercially available by NGK Insulators Ltd. in 2000.[88] Recently, increasing research has been made to realize the application of solid electrolytes. In particular, increasing attention has been turned from purely inorganic SSEs or purely organic SPEs to CSSEs. The research of these CSSEs has been focused on designing innovative superionic conductors, understanding the ion transport mechanism at the interface, and improving the electrochemical performance based on CSSEs. In the following sections, a comprehensive introduction to different CSSEs, including polymer-based, oxide-based, hydride-based, sulfide-based and halide-based CSSEs, will be presented and discussed.

Polymer-based CSSEs

Since 1973, significant attention has been paid to SPEs owing to their ease of synthesis, low shear modulus, low cost, compatibility with large-scale manufacturing processes and inherent mechanical toughness. However, SPEs exhibit a low oxidation voltage and poor thermal stability. Additionally, SPEs show particularly low ionic conductivity (10^{-6} to 10^{-8} S cm^{-1}) at room temperature because the polymer chains are locked in a crystal lattice which hinders ion-pair dissociation. Improvements in ionic conductivity and interfacial resistance between the electrolyte and electrodes are still unable to satisfy the requirements for practical applications. To address these problems, various physical approaches and chemical strategies, such as polymer–inorganic material blending, architectural design of inorganic fillers, copolymerization, crosslinking and the introduction of ionic side groups, have been adopted.

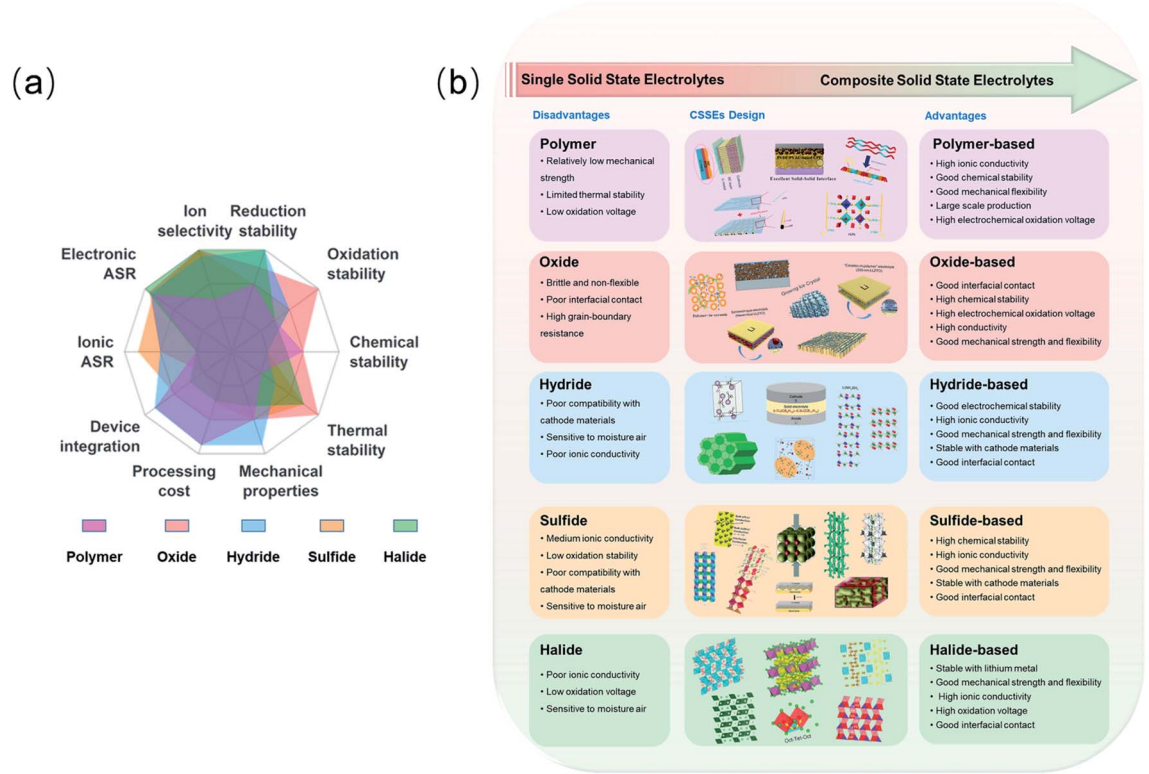

Fig. 1 (a) The superposed radar plot of different types of SSEs and requirements for SSEs. ASR, area-specific resistance. Reproduced from ref. 11 with permission from Springer Nature, copyright 2017. (b) Design of CSSEs from single type SSEs and corresponding physicochemical characteristics.

Researchers began to invest more effort to balance electrochemical stability and mechanical robustness in the development of composite polymer electrolytes (CPEs). The ionic conductivities of composite membranes were optimized as the content of $Li_7La_3Zr_2O_{12}$ changes. The composite membranes exhibited the highest ionic conductivity (4.42×10^{-4} S cm^{-1} at 55 °C) and maintained mechanical flexibility, consisting of an organic PEO matrix with the optimum composition (52.5% $Li_7La_3Zr_2O_{12}$).[89] In contrast to conventional blending methods, Cui *et al.* reported a new approach for the preparation of ceramic–polymer electrolytes *via in situ* synthesis of ceramic filler particles in polymer electrolytes. The improved distribution of monodisperse ultrafine SiO_2 particles in PEO helped increase the effective surface area and suppress the crystallization of PEO, thus facilitating polymer segmental motion for ionic conduction. All of these factors led to good ionic conductivity (1.2×10^{-3} S cm^{-1} at 60 °C, 4.4×10^{-5} S cm^{-1} at 30 °C) and greatly extended the electrochemical stability window up to 5.5 V.[90] Chung *et al.* reported a novel composite electrolyte fabricated by a simple solution casting method. The composite electrolyte ($Li_{6.4}La_3Zr_{1.4}Ta_{0.6}O_{12}$ (LLZTO) fillers in a PEO/$LiClO_4$ matrix) exhibited low interfacial resistance and good Li-ion conductivity (4.8×10^{-4} S cm^{-1} at 60 °C).[91]

Li^+-conducting oxides are considered better fillers than Li^+-insulating oxides for improving Li^+ conductivity and distribution in a composite electrolyte. To explore this possibility, a PEO/perovskite $Li_{3/8}Sr_{7/16}Ta_{3/4}Zr_{1/4}O_3$ (LSTZ) electrolyte was prepared. An interphase layer was *in situ* formed during cycling with the electrolyte membrane, which indicated the strong interaction between F^- and the surface Ta^{5+}. This strong interaction improved Li-ion transport at the PEO/perovskite interface and suppressed lithium dendrite growth.[92] More recently, Goodenough *et al.* used two Li^+-insulating oxides, fluorite $Gd_{0.1}Ce_{0.9}O_{1.95}$ (GDC) and perovskite $La_{0.8}Sr_{0.2}Ga_{0.8}Mg_{0.2}O_{2.55}$ (LSGM), as ceramic fillers in the PEO matrix. Density functional theory (DFT) calculations and ^{7}Li nuclear magnetic resonance (NMR) measurements confirmed the interaction between the oxide surface and the Li-salt anion in the polymer, which modified the activation energy for Li^+ transport to obtain a high Li^+ conductivity that was above 10^{-4} S cm^{-1} at 30 °C.[93] Cui *et al.* reported the facile synthesis of Al^{3+}/Nb^{5+} co-doped $Li_7La_3Zr_2O_{12}$ (LLZO) nanoparticles. The substitution of Li^+ by Al^{3+} enhanced the stabilization of cubic LLZO at RT, and the substitution of Zr^{4+} by Nb^{5+} improved the ion conductivity. After optimization, the polymer electrolyte with 15 wt% LLZO showed an improved conductivity of 9.5×10^{-6} and 1.1×10^{-4} S cm^{-1} at 20 and 40 °C, respectively.[94] There was a higher Li-ion conductivity in one/two-dimensional fillers than in zero-dimensional particles. One-dimensional $Li_{0.33}La_{0.557}TiO_3$ (LLTO) nanofiber embedded in a PEO matrix, as shown in Fig. 2a–c, provided continuous ionic transport pathways and reduced interfacial resistance.[95] Moreover, two-dimensional garnet nanosheets were first reported *via* co-precipitation with a graphene oxide (GO) template. The specially designed CPE containing garnet nanosheets could robustly isolate Li

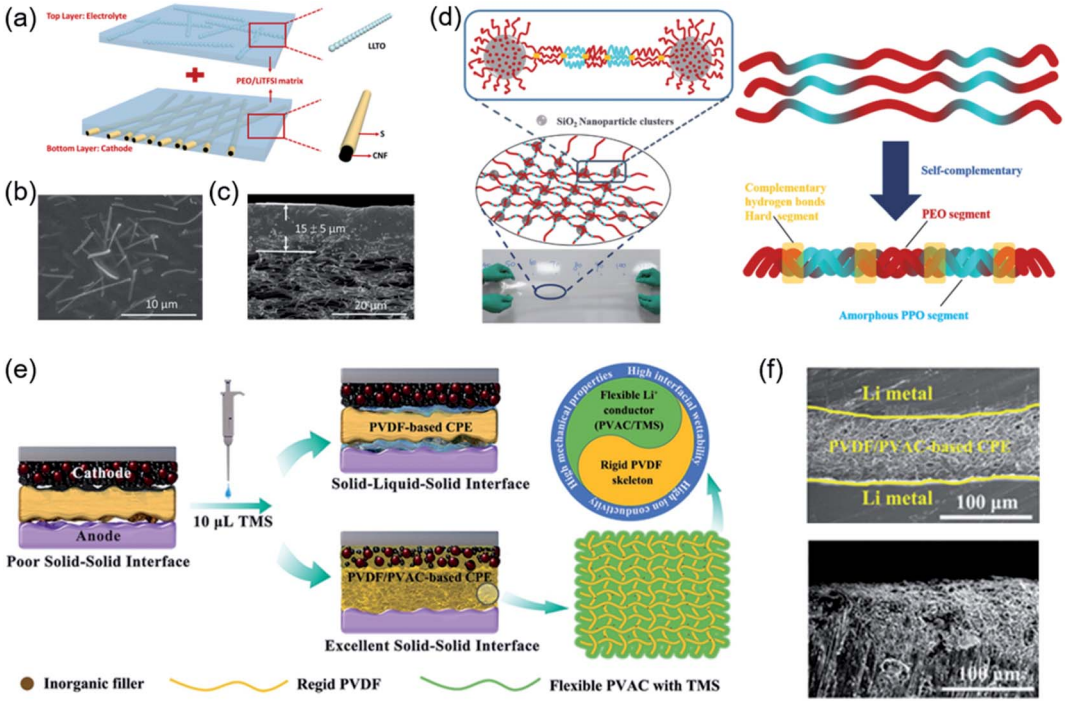

Fig. 2 (a) Schematic illustration of the carbon nanofiber (CNF)/S-PEO/LLTO CSSE. (b) SEM images and (c) cross-sectional SEM image of the PEO/LLTO CSSE. Reproduced from ref. 95 with permission from Elsevier Inc., copyright 2019. (d) Graphical representation of the 3D framework in cross-linked nanocomposite polymer electrolytes (CNPEs). Reproduced from ref. 97 with permission from Elsevier Inc., copyright 2020. (e) Schematic illustration of the different interfacial characteristics between the PVDF-based CPE and PVDF/PVAC-based CPE. (f) Cross-sectional SEM images of the symmetric battery and Li metal after Li plating/stripping 200 h. Reproduced from ref. 101 with permission from Wiley-VCH, copyright 2020.

dendrites and exhibited a conductivity of 3.6×10^{-4} S cm^{-1} at RT.[96]

Currently, the general strategies are adding integrated inorganic fillers to the SPE matrix or preparing polymer electrolytes with specific intermolecular interactions, which can not only improve the ionic conductivity but also sustain a high working voltage. Mai *et al.* provided a new approach to prepare cross-linked nanocomposite polymer electrolytes based on hydrophobic–hydrophilic–hydrophobic triblock copolymers (PPO–PEO–PPO) in Fig. 2d. In this enhanced framework, polymer-based composite electrolytes were generated from copolymers and surface-modified SiO_2 nanoparticles, which led to the effective solvation of lithium salts and encapsulation of organic solvents. Thus, the electrolytes exhibited high ionic conductivity and their electrochemical stability window was extended to 6.5 V.[97] The experiments, together with theoretical calculations, demonstrated that the gas releasing behaviour of PEO may be ascribed to the high oxidizing ability of delithiated $LiCoO_2$. PEO was reported to decompose and release oxygen from $LiCoO_2$ when more than $0.5Li^+$ was removed.[98] The surface catalytic effect of delithiated $LiCoO_2$ caused oxidation/dehydration of PEO-based SPBs and unexpected H_2 generation at 4.2 V. To mitigate the surface catalytic effect, the surface of $LiCoO_2$ was coated with a stable solid electrolyte $Li_{1.4}Al_{0.4}Ti_{1.6}(PO_4)_3$ (LATP), thus avoiding direct contact with PEO and therefore extending the stable working voltage to over 4.5 V.[99] Park *et al.* synthesized a self-standing and flexible CPE through the introduction of poly-(ethylene glycol)-dimethyl ether (PEGDME) to be plasticized in a PEO matrix with a uniformly distributed ceramic filler. After the addition of PEGDME, the stable working voltage of the PEO matrix was extended to 5.0 V.[100] Besides PEO-based polymer electrolytes, a PVDF/polyvinyl acetate (PVAC)/LLZTO CPE was first fabricated to achieve high RT ionic conductivity and a high electrochemical stability window (4.5 V) (Fig. 2e). More importantly, the intermolecular interactions of tetramethylene sulfone (TMS) combined with PVAC or PVDF showed distinct differences. The Li/PVDF/PVAC-based CPE/Li symmetric battery shows a good inhibition of lithium dendrite growth in Fig. 2f. The PVAC/TMS layer formed on both the cathode and anode interfaces constructed an effective sulfurous Li^+ transport pathway. Therefore, TMS with low flammability and excellent stability was able to selectively interact with only PVAC, which was helpful to enhance lithium-ion conductivity and electrode/electrolyte interfacial compatibility.[101]

Recently, sulfide electrolytes, such as Li_2S–GeS_2, $Li_2SeP_2S_5$, $Li_2SeB_2S_3$ and Li_2SeSiS_2, have attracted increasing attention due to their superior ion conductivity ($\sim 10^{-2}$ S cm^{-1}) and wide potential window (>10 V). Furthermore, sulfide electrolytes have cheaper precursors and simpler processes to provide the electrolyte with a large potential in all-solid-state lithium batteries (ASSLBs). However, little success has been achieved in adopting lithium metal anodes with sulfide-based electrolytes in ASSLBs. The main challenges are the interfacial instability and Li dendrite formation between Li metal and SSEs.

To solve these issues, $Li_{10}GeP_2S_{12}$ (LGPS) was dispersed in a PEO-based polymer to fabricate SPE membranes. The inorganic LGPS in the organic PEO matrix impeded crystallization and weakened the interactions between the Li^+ and PEO chains. The optimal SPE containing 1% LGPS electrolyte exhibited a maximum ionic conductivity of 1.21×10^{-3} S cm^{-1} at 80 °C and a broadened electrochemical window up to 5.7 V.[102] Inspired by the similarity between the H bond and Li bond, hybrid solid electrolytes were prepared *via* an *in situ* coupling reaction. A commercialized silane coupling agent was used as a bridge builder to realize the chemical bonding interaction between LGPS, polyethylene glycol (PEG), and PEO (Fig. 3a and b). Hence, the optimal ceramic/polymer hybrid solid electrolyte (HSE) membrane provided an expressway for the transport of Li^+, and the growth of lithium dendrites was suppressed.[103] Li_6PS_5Cl is a promising solid electrolyte in ASSLBs. In the preparation process, S and Cl easily formed chemical bonds with the polymer groups and replaced other anion sites.[104] A Li_6PS_5Cl/PEO composite electrolyte with enhanced mechanical properties and a stable interface was fabricated by a liquid-phase process. In particular, with an optimal value of 5 wt% PEO, the CSEs show an improved ionic conductivity and electrochemical window.[105] Sun *et al.* reported a plastic crystal electrolyte (PCE) interlayer to address the interfacial challenge and lithium dendrite formation between sulfide electrolytes and Li metal. Using PCE as an interlayer, interfacial reactions could be avoided by preventing contact between the sulfide electrolytes and Li metal (Fig. 3c–e). In addition, submerging the cathode in a PCE matrix forms a continuous 3D-conduction pathway for Li^+ on the cathode side.[106] The synchrotron-based X-ray absorption spectra in Fig. 3e were used to analyze the interface between LGPS and Li metal, which suggests that using the PCE interlayer can prevent the reduction of LGPS by Li metal.

Oxide-based CSSEs

Oak Ridge Laboratory first synthesized LiPON in the 1990s.[107] Since then, oxide electrolytes have attracted increasing attention. Compared to SPEs, oxide-based electrolytes are becoming a research hotspot owing to their chemical stability in air, good ion selectivity and wide electrochemical window.[15] Unfortunately, an increasing number of studies have demonstrated that lithium dendrites occur in most oxide-based electrolytes owing to poor interfacial stability, large interfacial resistance and voids and cracks inside the electrolytes. To develop an interface with chemical and mechanical stability, researchers have adopted interfacial engineering by introducing artificial buffer layers to protect these SSEs against lithium dendrite growth.[108,109] Nevertheless, simple physical contact could not

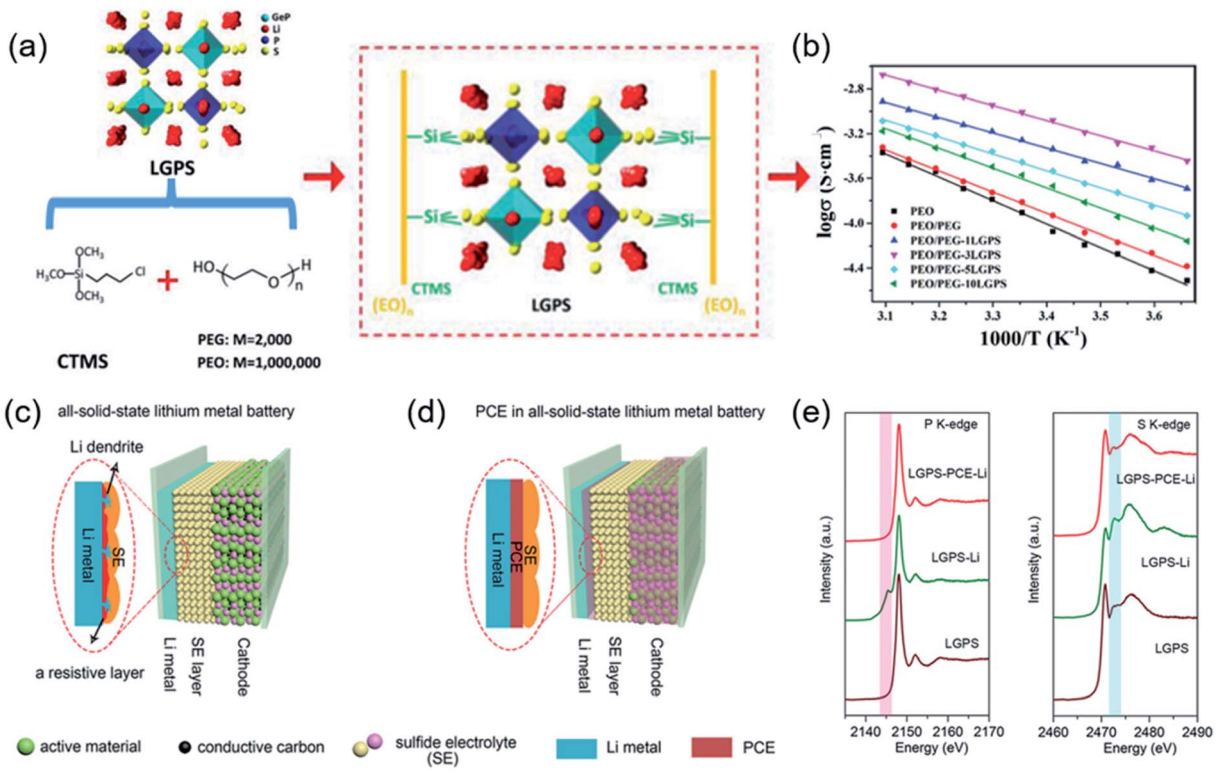

Fig. 3 (a) Schematic illustration of the as-prepared HSE structure. Electrochemical characterization of the HSE membranes. (b) Arrhenius plot of different electrolytes from 0 to 50 °C. Reproduced from ref. 103 with permission from Wiley-VCH, copyright 2020. Schematic diagrams of (c) ASSLMBs and (d) ASSLMBs with the PCE interlayer. X-ray absorption (e) P K-edge and S K-edge spectra of LGPS before cycling, LGPS on the Li surface after cycling, and LGPS with the PCE interlayer after cycling, respectively. Reproduced from ref. 106 with permission from Wiley-VCH, copyright 2019.

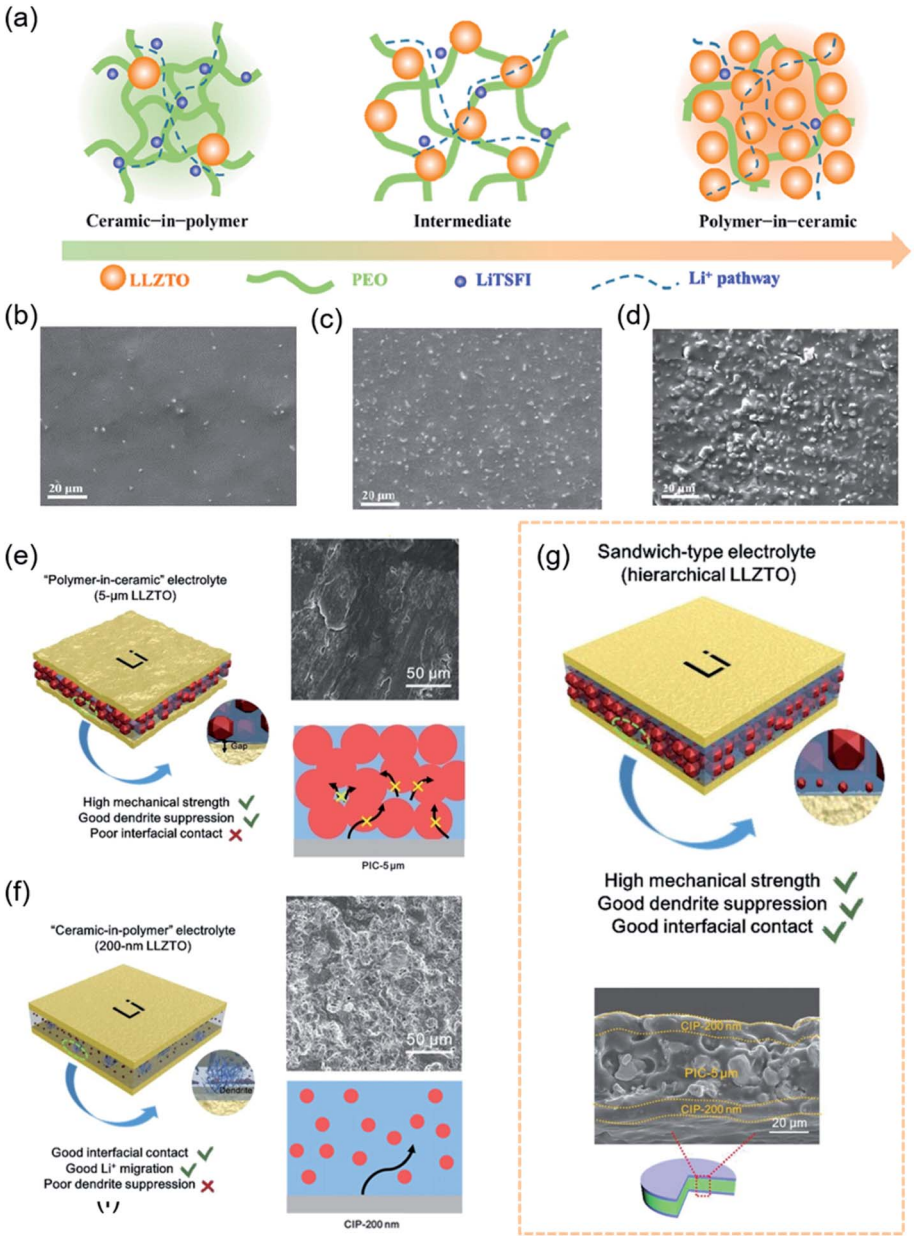

Fig. 4 (a) Schematic illustration of PEO–LLZTO CSSE: "ceramic-in-polymer"; "intermediate"; "polymer-in-ceramic", and corresponding (b–d) SEM images. Reproduced from ref. 56 with permission from Elsevier Inc., copyright 2018. The schematic illustrations of (e) PIC-5 μm, (f) CIP-200 nm, and (g) hierarchical sandwich-type CSSEs, and corresponding SEM images. Reproduced from ref. 114 with permission from Wiley-VCH, copyright 2019.

solve the problems of large area specific resistance and dendrite formation. Due to a high shear modulus, the problem of interfacial contact was initially solved by designing a soft interface, such as polymer layers, amorphous oxides and metal coatings.[110–112]

In practice, Ding *et al.* demonstrated that the coating layer of PEO (LiTFSI) could effectively prevent side reactions between the $Li_{1.5}Al_{0.5}Ge_{1.5}(PO_4)_3$ (LAGP) and Li anode.[113] It was exciting that the CSSE remained stable even at a high potential of 5.12 V. Considering the excellent performance of the polymer layer, Goodenough *et al.* developed a low-cost composite ceramic/polymer solid-state electrolyte (CPSE) containing up to 80 wt% garnet $Li_{6.4}La_3Zr_{1.4}Ta_{0.6}O_{12}$ (LLZTO).[56] Composites consisting of compositions ranging from "ceramic-in-polymer" to "polymer-in-ceramic" were found to be flexible and mechanically robust (Fig. 4a–d). The crystalline LLZTO particles not only increased the chain segment motion in a PEO matrix but also afforded an alternative Li^+-conduction pathway. Compared with the "ceramic-in-polymer" electrolyte with high flexibility, the "polymer-in-ceramic" electrolyte was more suitable for large-scale application in electric vehicles owing to its high mechanical strength and safety. The PEO–

LLZTO composite electrolyte showed the highest ionic electrolyte conductivity (above 10^{-4} S cm^{-1} at 55 °C) and suppressed Li dendrite growth. Coincidentally, to design an effective approach to achieve dendrite-free CSSEs, Sun *et al.* investigated the performance of composite electrolytes from "ceramic-in-polymer" to "polymer-in-ceramic" (Fig. 4e–g).[114] The different sizes of garnet particles embedded in the electrolyte improved ionic conductivity and tensile strength. The satisfactory sandwich-type composite electrolyte with hierarchical garnet particles simultaneously achieved dendrite suppression and excellent interfacial contact with the Li metal in Fig. 4g. The "polymer-in-ceramic" interlayer with 80 vol% 5 μm LLZTO showed a high mechanical strength of 12.9 MPa and hindered Li dendrite propagation due to physical obstacles. The "ceramic-in-polymer" thin-film outer layers with 20 vol% 200 nm LLZTO particles created a smooth and flexible surface with a high t_+ (Li^+ transference number) of 0.47. Symmetric solid-state cells with Li maintained highly stable plating/stripping cycling for 400 h under 0.2 mA cm^{-2} at 30 °C. Full SSBs with a $LiFePO_4$ cathode and Li metal anode delivered a RT specific capacity of 99.1 mA h g^{-1} with a good capacity retention of 82.4% after 200 cycles at 0.1C.

The design of artificial structures can not only be beneficial for interfacial contact but also improve mechanical properties. Composite electrolytes with high loadings of ceramic fillers (>50 vol%) are necessary to achieve the required mechanical modulus.[115] However, high loading can lead to a large interparticle contact resistance and insufficient particle–particle contact area, thus resulting in greatly decreased ionic conductivity. Therefore, designing a composite with an interconnected ceramic network takes advantage of the high ionic conductivity of the ceramic. Inspired by the structure of natural nacre, Yang *et al.* fabricated a "brick-and-mortar" arrangement of solid electrolytes with ceramic electrolyte microplatelets as the "brick" and polymer electrolytes as the "mortar" (Fig. 5a and b).[116] Compared to pure ceramic electrolytes, the nacre-like ceramic/polymer composite electrolyte simultaneously exhibited high fracture strain and an ultimate flexural modulus to accommodate external deformation. The staggered microstructure provided a high fracture strain of 1.1% and a flexural modulus of 7.8 GPa. An ice template method was used to build a vertically aligned ceramic/polymer composite electrolyte (Fig. 5c and d), which was composed of LAGP, with a high ionic conductivity, and PEO.[117] The vertical LAGP walls in the polymer

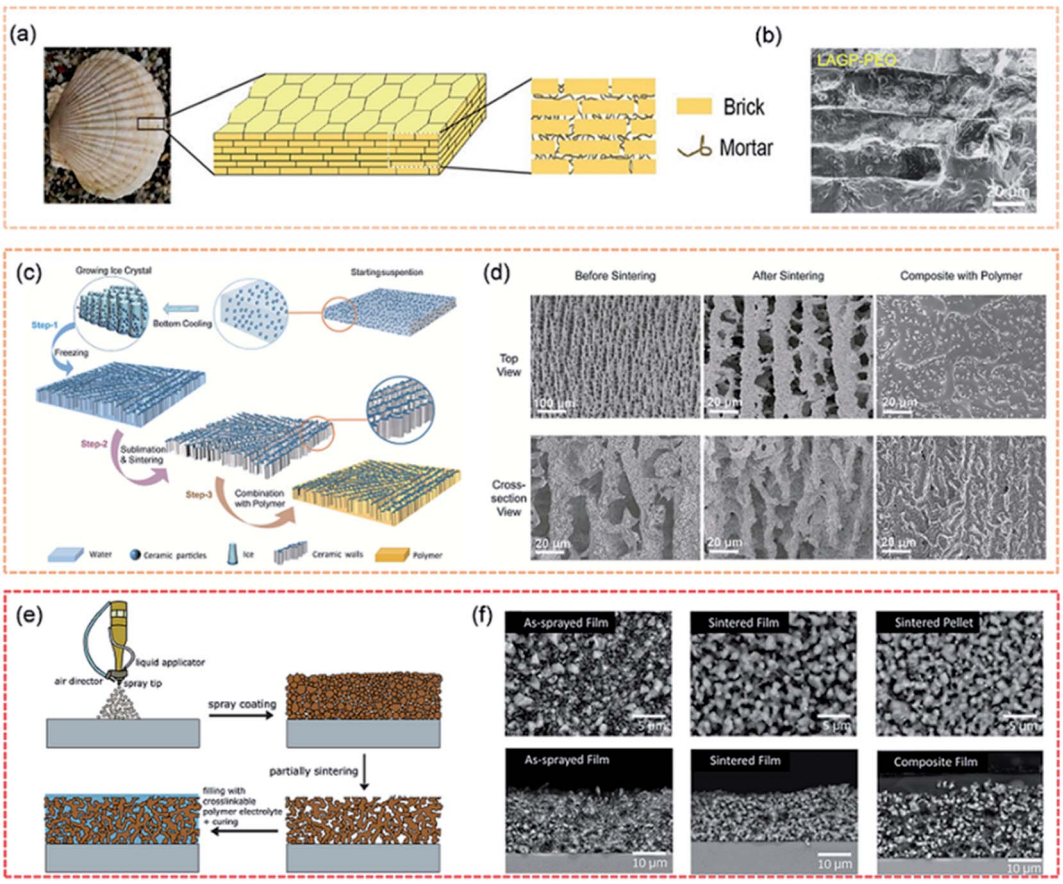

Fig. 5 (a) Schematic of the staggered "brick-and-mortar" microstructure of the LAGP–PEO NCPE film, and the corresponding (b) cross-sectional SEM image. Reproduced from ref. 116 with permission from Wiley-VCH, copyright 2020. (c) The schematic of the preparation process of the ice-templated LAGP/PEO CSSE, and the corresponding (d) SEM images. Reproduced from ref. 117 with permission from Elsevier Inc., copyright 2019. (e) Schematic illustration of the fabrication procedure of the composite electrolyte film, and the corresponding (f) SEM images. Reproduced from ref. 118 with permission from Elsevier Inc., copyright 2020.

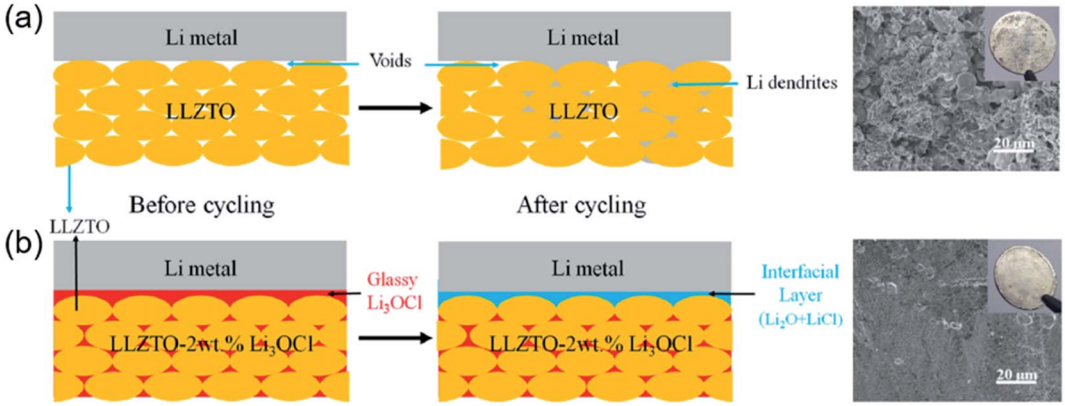

Fig. 6 Schematics of Li deposition behavior using (a) LLZTO SSE and (b) LLZTO–2wt% Li_3OCl CSE. Reproduced from ref. 126 with permission from Elsevier Inc., copyright 2018.

provided fast ionic transport channels while retaining matrix flexibility. The ideal structure maximized the ionic conductivity of the composite electrolyte (1.67×10^{-4} S cm^{-1} at RT and 1.11×10^{-3} S cm^{-1} at 60 °C). In Chen's work, a composite solid electrolyte with a 3D-interconnected ceramic network was fabricated using a readily scalable processing method, as shown in Fig. 5e and f.[118] The composite electrolyte had high ceramic loadings (77 wt% and 61 vol%) and demonstrated high ionic conductivity (3.5×10^{-5} S cm^{-1} at RT) as well as good mechanical strength (19.5 MPa).

In addition to excellent performance, the cost of processing should be considered in practical applications. Oxide electrolytes with superior ionic conductivity are synthesized at a high temperature, increasing the cost of the preparation process as well as the risk to the operation process.[119] Therefore, developing a feasible method to address energy consumption and safety issues is reasonably significant for SSEs in practical applications. Liquid-phase sintering additives have received considerable attention because they have a low melting point and form a liquid phase. Li-based glass ceramics, such as Li_2O, Li_3BO_3 (LBO), and $LiSiO_4$, are utilized for densifying LLZO at low temperatures.[120–123] In addition to borate electrolytes, halide electrolytes Li_3OX (X = Cl and Br) also display good electrochemical stability with Li metal and a low melting temperature ($T_m \approx 282$ °C).[124,125] Taking advantage of the above merits, Li_3OCl was introduced into the voids and boundaries of Ta-doped $Li_{6.75}La_3Zr_{1.75}Ta_{0.25}O_{12}$ (LLZTO) particles at 350 °C (Fig. 6). In LLZTO–$x$$Li_3OCl$ CSSEs, amorphous Li_3OCl, as a binder, filler and bridge, promoted the formation of an integrated continuous ion-conductive network among the LLZTO particles. Furthermore, Li_3OCl, with excellent affinity, *in situ* reacted to form

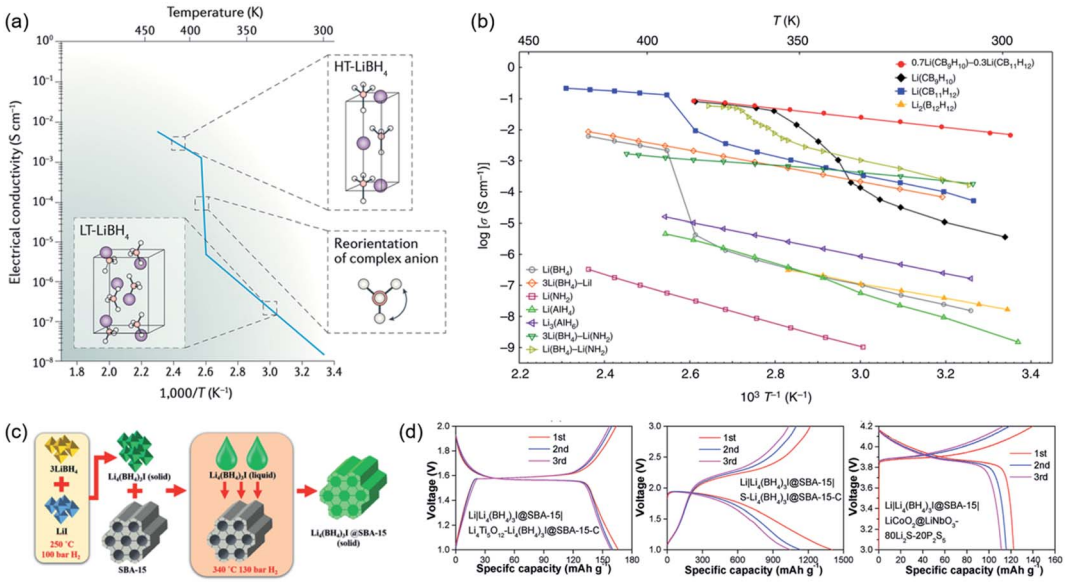

Fig. 7 (a) Structural transition of $LiBH_4$ from low temperature to high temperature phases triggered by the reorientation of complex anions. Reproduced from ref. 127 with permission from Springer Nature, copyright 2016. (b) Li^+ ionic conductivity in complex hydrides. Reproduced from ref. 84 with permission from Springer Nature, copyright 2019. (c) Schematic diagram of the synthetic process of $Li_4(BH_4)_3I$@SBA-15. (d) Full cell test based on the $Li_4(BH_4)_3I$@SBA-15 composite electrolyte. Reproduced from ref. 135 with permission from Wiley-VCH, copyright 2019.

a stable and dense interfacial layer, which greatly decreased the interfacial resistance (from 1850 to 90 Ω cm^2) and effectively suppressed lithium dendrite growth. The integrated CSSEs (LLZTO–2wt% Li_3OCl) with compact and stable structures presented optimal ionic conductivity (2.27×10^{-4} S cm^{-1}), and their electrochemical stability window was up to 10 V at RT.[126] The above studies highlighted a novel strategy for developing integrated and compact CSSEs at ultralow temperature for high-performance ASSLBs.

Hydride-based CSSEs

In contrast to oxide and polymer SSEs, hydride SSEs belong to the complex hydride family and have been widely investigated as solid-state hydrogen-storage materials.[127,128] To date, there has been little research on ionic conduction in complex hydrides owing to their poor ionic conductivity at moderate temperatures. In 2007, $LiBH_4$ was reported as a fast-ion conductor by Orimo *et al.*, and this is regarded as a turning point in the development of hydride SSEs.[73] The ionic conductivity dramatically jumped by 3 orders of magnitude from 10^{-7} S cm^{-1} (303 K) to 10^{-3} S cm^{-1} (393 K), accompanied by a structural transition from orthorhombic to hexagonal (Fig. 7a).[129] Furthermore, no polarization has been detected at the $LiBH_4$–Li metal interface due to good reduction stability and low grain boundary resistance. The interfacial stability was even tested under a high current density of 2.8 mA cm^{-2}.[130] However, the fast 2D-Li^+ conduction phenomenon could only occur in the high-temperature phase, which was a serious constraint for applying hydride SSEs in practical solid-state batteries. To improve the ionic conductivity of orthorhombic $LiBH_4$ or prepare RT-stabilized hexagonal $LiBH_4$, great efforts have been made, such as second-phase compositions, anion doping, and interfacial modifications. Therefore, a series of CSSEs have been synthesized based on hydrides.[71]

A larger ionic radius (such as I^-, 0.220 nm) can help increase the distance between alkali-metal ions and $[BH_4]^-$ ions, which exhibit a low transition temperature.[74] With efforts to obtain high conductivity at moderate temperature, the concept of partially replacing $[BH_4]^-$ complex ions with I^- ions was proposed and investigated. Among these conceptual materials,

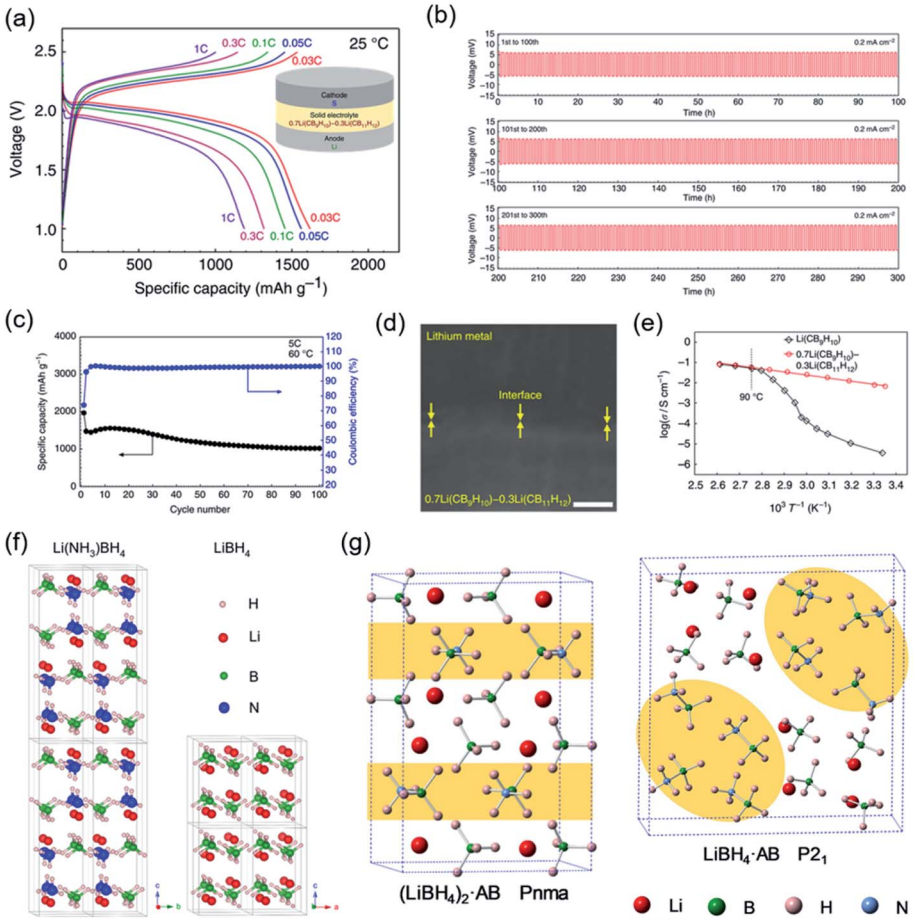

Fig. 8 (a) Discharge–charge profiles at 298 K. (b) Stability of the composite electrolyte with lithium metal. (c) Cycling performance of the *closo*-type complex hydride-based Li–S battery. (d) FE-SEM image of the electrolyte/Li interface. (e) Ionic conductivity properties. Reproduced from ref. 84 with permission from Springer Nature, copyright 2019. (f and g) Crystal structures of $Li(NH_3)BH_4$, $LiBH_4$, $(LiBH_4)_2AB$, and $LiBH_4AB$. Reproduced from ref. 76 and 142 with permission from Elsevier Inc., copyright 2018 and permission from American Chemical Society, copyright 2019.

a $LiBH_4$–LiI system was proven to be the most successful due to showing a high Li^+ conductivity in the order of 10^{-5} S cm^{-1} for $3LiBH_4$–LiI at RT (Fig. 7b). No significant structural change was observed from differential scanning calorimetry (DSC) profiles, which revealed good structural stability and thermodynamic properties of the composite electrolyte.[131] After a halide modification, the stability against Li was demonstrated by SEM and Li plating/stripping experiments. An all-solid-state Li–S battery with a $3LiBH_4$–LiI electrolyte exhibited high reversible capacity.[132] Afterwards, researchers found that nanoconfined $LiBH_4$ in the pores of ordered mesoporous silica scaffolds led to high Li^+ conductivity due to the fast Li^+ mobility at the interface between $LiBH_4$ and SiO_2.[72,133,134] The above result also led to a lower phase transition temperature than for bulk $LiBH_4$. More recently, inspired by the success of hydride–halide composites and nanoconfinement through mesoporous materials, $Li_4(BH_4)_3I$ was nanoconfined into SBA-15 *via* a two-step process by Zheng *et al.*(Fig. 7c and d).[135] $Li_4(BH_4)_3I$@SBA-15 exhibited a high conductivity of 2.5×10^{-4} S cm^{-1} at 35 °C with a Li-ion transference number of 0.97. Furthermore, the formation of a stable SEI between Li and the electrolyte could effectively suppress the growth of Li dendrites. More significantly, the good compatibility of $Li_4(BH_4)_3I$@SBA-15 for ASSLBs was investigated with different cathodes, *i.e.*, $Li_4Ti_5O_{12}$, S and $LiCoO_2$. On the other hand, the origin of dendrite growth in $LiBH_4$ was clarified by Sun *et al.* in 2019. Li^+ combines with electrons within the grain boundary/pore of the SSE, reducing to Li^0 and eventually leading to a short circuit. Herein, the electronic conductivity of SSEs plays a significant role in dendrite formation. In this case, LiF was employed as an insulator for the $LiBH_4$ SSE. The $LiBH_4$–LiF CSSE exhibited amazing stability at 5.0 mA cm^{-2} for over 200 cycles, successfully inhibiting the growth of Li dendrites.[130]

A low activation energy is also needed to obtain a superionic conductor.[136] For example, the E_a of 0.46 eV for $Li_4(BH_4)_3I$@SBA-15 was lower than that of 0.56 eV for $Li_4(BH_4)_3I$, which contributed to the high conductivity of the former. Thus, to weaken the electrostatic interaction between Li^+ and $[BH_4]^{1-}$, sulfide materials were introduced into $LiBH_4$ to form a hybrid system.[137] A pseudo-binary system composed of a complex hydride and sulfide was reported by Orimo *et al.* in 2016.[138] A new crystalline phase of $90LiBH_4$:$10P_2S_5$ with a possible orthorhombic structure was achieved with a high ionic conductivity of $\log(\sigma/S\ cm^{-1}) = -3.0$ at 300 K. A lower E_a for the new structure was calculated to be 0.38 eV compared with 0.53 eV for HT-$LiBH_4$. A smooth charge transfer between the SSE and TiS_2 electrode was certified to occur through a charge/discharge process. Unlike single complex hydrides, the new composite electrolyte exhibited no phase transition before 473 K and a wide electrochemical window of 0–5 V. Hydride-based CSSEs also experience stability issues as many candidates decompose on the cathode side.[139] Many approaches have been developed to enhance the interfacial stability of CSSEs against cathodes, such as designing stable interfaces between the hydride SSEs and cathodes. To accommodate high-voltage cathodes, such as commercial $LiCoO_2$, sulfides have recently been introduced to decrease the interfacial resistance between $LiCoO_2$ and hydride-based SSEs by forming a stable Li-ion conductive cathode electrolyte interphase (CEI) layer.[135,140] These hydride-based CSSEs can work well in all-solid-state LIBs with a $LiCoO_2$ cathode, which exhibits typical high-voltage plateaus for charge/discharge.

Additionally, a novel SSE from a solid solution of two *closo*-type complex hydrides, videlicet $0.7Li(CB_9H_{10})$–$0.3Li(CB_{11}H_{12})$, was reported with a high ionic conductivity of over 10^{-3} S cm^{-1} at 298 K (Fig. 8a–e).[84] High stability against lithium metal was certified by lithium plating/stripping for 300 cycles with an extremely stable lithium-ion transfer capability at 0.2 mA cm^{-2}. Based on a cathode loading of 2.5 mg cm^{-2}, all-solid-state Li–S batteries (ASSLSBs) presented a good reversible capacity of 1239 mA h g^{-1} after 20 cycles at 1C (298 K); the notable energy densities were calculated to be over 2500 W h kg^{-1} at high current densities (1–3C). Moreover, based on the SEM observation it was found that dendrite growth was suppressed at the interface between $0.7Li(CB_9H_{10})$–$0.3Li(CB_{11}H_{12})$ and Li metal. Overall, these CSSE-based SSLSBs exhibited outstanding electrochemical performance at 298 K. Alternatively, approaches to improve the conductivity of $LiBH_4$-based composites in regard to inducing defects and changing the atomic arrangement have been attempted. To decrease the volume density of Li ions in $LiBH_4$, neutral molecules were brought into $LiBH_4$. This new concept was first achieved by the utilization of ammonia absorption into $LiBH_4$, leading to a structural transition and reducing the activation energy of Li-ion mobility (Fig. 8f).[76] $Li(NH_3)_nBH_4$ ($0 < n \leq 2$) exhibited high ionic conductivity (2.21×10^{-3} S cm^{-1}). A drastic increase in ionic conductivity occurred at approximately 37 °C, which is close to human body temperature, which shows its potential to be utilized in wearable devices. More recently, the Li^+-conduction mechanism in $LiBH_4 \cdot 1/2(NH_3)$ was systematically investigated through crystal structure analysis and DFT calculations by Jensen *et al.*[141] The molecular volume of NH_3BH_3 ($v = 69.86$ Å^3 per unit cell) was much larger than that of NH_3 ($v = 37.79$ Å^3 per unit cell), which would intrinsically increase the cell volume of $LiBH_4$ and lower the volume density of Li ions (Fig. 8g). Remarkably, a novel RT ultrafast CSSE ($LiBH_4 \cdot NH_3BH_3$) was demonstrated with a conductivity up to 4.04×10^{-4} S cm^{-1} at 298 K.[142]

In short, the formation of composites with other materials can effectively promote high ionic conductivity in $LiBH_4$. Additionally, the original shortcomings of hydride-based SSEs, such as the ionic area specific resistance, thermal stability of composites, and oxidation stability with cathodes, have been overcome accordingly. Inspired by these studies, other nano/composites have been investigated, *e.g.*, 2.0×10^{-5} S cm^{-1} for the $LiBH_4$–C_{60} composite at 298 K.[143] There are also several reports on ionic conductivities in hydride–nitride/imide systems,[144] including but not limited to a $LiBH_4$–Li_3N system[145] and a $LiBH_4$–Li_2NH system.[146]

Sulfide-based CSSEs

By replacing oxygen ions with sulfur ions, owing to their lower electronegativity and larger radius, sulfide SSEs present a weaker bonding strength between the sulfur and lithium ions

and provide a wider migration tunnel for lithium ions. As a result, sulfide SSEs exhibit higher ionic conductivities, approximately 10^{-3} to 10^{-4} S cm^{-1} at RT, which are almost comparable to those of liquid electrolytes. In 1986, Li_2S–SiS_2 was first synthesized by twin roller quenching.[147] Then, through further doping with a Li_3PO_4 electrolyte, the conductivity increased to 0.69×10^{-3} S cm^{-1}.[148] In 2011, a thio-lithium superionic conductor (thio-LISICON) $Li_{10}GeP_2S_{12}$ was first reported to have a high ionic conductivity of 1.2×10^{-2} S cm^{-1} at RT (Fig. 9a), which greatly promoted the development of sulfide SSEs.[16] To improve conductivity, the same group discovered a novel lithium superionic conductor, $Li_{9.54}Si_{1.74}P_{1.44}S_{11.7}Cl_{0.3}$, based on a double substitution with aliovalent-ion doping (Fig. 9b).[10] An exceptionally high conductivity of 2.5×10^{-2} S cm^{-1} was obtained.

However, under current laboratory conditions, the cell-based energy density of ASSLBs is much lower than that of their competitors with liquid electrolytes. Because of the brittleness of electrolyte materials, the thickness of the electrolyte layer is often more than 1 mm to avoid the formation of cracks during high pressure stress.[149] Synthesizing a sulfide/polymer composite electrolyte is an effective method to slim the electrolyte layer and maintain a high ionic conductivity. Kanno *et al.* prepared a thio-LISICON/silicone composite electrolyte sheet.[150] Recently, an increasing number of compliant sulfide–polymer composite electrolytes have been successfully developed. Whiteley *et al.* produced a 64 μm-thick membrane with a sulfide loading of 77 wt% that exhibited a low shear modulus and high ionic conductivity of 10^{-4} S cm^{-1} at RT (Fig. 9c). An ultrathin solid-state membrane (100 μm) was fabricated based on $77.5Li_2S$–$22.5P_2S_5$ with a self-healing polymer matrix. It was applied as a separator (80 wt%) in ASSLBs with an FeS_2-based cathode and achieved excellent rate capability and stable cycling for over 200 cycles.[151] More recently, Nan *et al.* prepared a free-standing composite solid electrolyte membrane with $78Li_2S$–$22P_2S_5$ concentrations from 80 to 97 wt%. The sulfide/PEO and sulfide/PVDF composites showed ionic conductivities of 4–7 $\times 10^{-4}$ S cm^{-1} with a thickness of 120 μm.[58] A moderate PEO content could help the composite electrolyte achieve good mechanical properties and a stable electrolyte/lithium interface.[105,152–155] For example, with 5 wt% PEO, the proportional limit of Li_6PS_5Cl composite solid electrolytes was enhanced to a value of 60 MPa. The as-assembled cell exhibited a good capacity retention rate of 91% over 200 cycles at 0.05C and 303 K. Further characterization indicated that lithium dendrite growth could be effectively inhibited after the PEO modification.[105] The formation of P–O–C bonds between the sulfide glass and oligomers was the key factor to ensure a high conductivity. It was also noted that the addition of small amounts of polymers improved ion conduction by lowering the glass transition temperature.[156]

In addition to combining with organic polymers, inorganic materials can act as fillers in sulfide-based electrolytes. Hood *et al.* reported the effect of oxide fillers in composites with β-Li_3PS_4 for the enhancement of the parent electrolyte. For example, 2 wt% Al_2O_3 increased the ionic conductivity of the parent electrolyte to 2.28×10^{-4} S cm^{-1} while maintaining electrochemical stability against metallic lithium up to 5 V.[157] Similarly, the same group examined the composite electrolyte of a "hard" oxide ($Li_7La_3Zr_2O_{12}$, LLZO) and a "soft" sulfide (β-Li_3PS_4, LPS), which demonstrated an excellent conductivity of 5.36×10^{-4} S cm^{-1} at 298 K; the above conductivity was higher

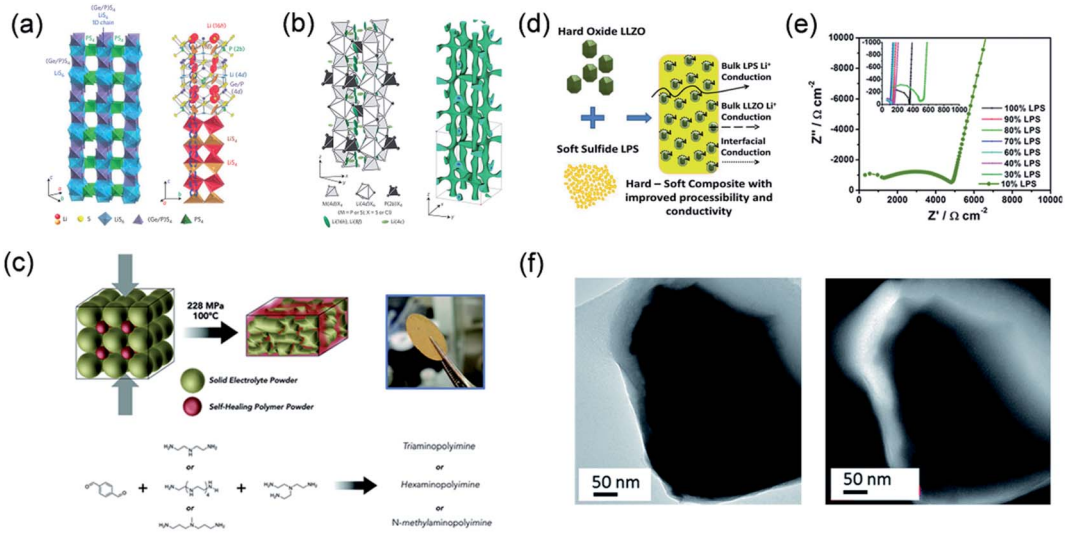

Fig. 9 (a) Framework structure of $Li_{10}GeP_2S_{12}$ and conduction pathways of lithium ions. Reproduced from ref. 13 with permission from Nature Publishing Group, copyright 2011. (b) Crystal structure of $Li_{9.54}Si_{1.74}P_{1.44}S_{11.7}Cl_{0.3}$ and nuclear distributions of Li atoms. Reproduced from ref. 7 with permission from Nature Publishing Group, copyright 2016. (c) Schematic of the formation of the solid electrolyte in a polymer matrix membrane. Reproduced from ref. 151 with permission from Wiley-VCH, copyright 2015. (d) Schematic illustration of the preparation process of the LPS–LLZO CSSE. (e) The ionic conductivity properties of the LPS:LLZO mixture. (f) TEM image of the LLZO–LPS composite electrolyte (the core–shell structure) and the EELS map show a higher Li concentration across the LLZO–LPS interface (the bright part has a high concentration of Li). Reproduced from ref. 158 with permission from the Royal Society of Chemistry, copyright 2014.

than that of its parent electrolytes (Fig. 9d and e). The improved conductivity was considered an effect of the space charge layer at the interface between the LLZO and LPS particles, which was believed to redistribute the ionic and electronic point defects (Fig. 9f).[158] As both sulfide and hydride SSEs are very sensitive to humid air, the handling process is always conducted in a glove box in an inert gas atmosphere. Due to the similarity of the chemical stability of these two types of electrolytes, a composite of hydride ($LiBH_4$) and sulfide (Li_3PS_4) showed the potential to improve the total lithium-ion conductivity. Tatsumisago *et al.* examined the effects of the addition of $LiBH_4$ on the structures and properties of sulfide electrolytes. The conductivities of the composite SSEs increased with increasing $LiBH_4$ content. The CSSEs had a wide electrochemical window up to 5 V *vs.* Li^+/Li^-. The glass with a composition of $2Li_3PS_4 \cdot LiBH_4$ showed the highest conductivity of 1.6×10^{-3} S cm^{-1} at RT.[159]

Halide-based CSSEs

To realize the application of ASSLBs at RT, current research efforts focus mostly on ionic conductivity and a wide electrochemical stability window. Compared to other SSEs, halide SSEs have had a relatively delayed development before 2018 because of their low ionic conductivity and low oxidation voltage.[160,161] With the tireless efforts of countless researchers, a large breakthrough in halide SSEs occurred in 2018.[68] Tetsuya Asano *et al.* successfully synthesized Li_3YCl_6 and Li_3YBr_6 with high ionic conductivities of 0.03–1.7 $\times$ 10^{-3} S cm^{-1} at RT.[68] Afterwards, other halide SSEs with high ionic conductivity, such as Li_3ErCl_6,[162,163] Li_3InCl_6 (ref. 70 and 164) and $Li_{3-x}M_{1-x}Zr_xCl_6$ (M = Y, Er),[165] were also successfully fabricated. In addition, recent experimental and theoretical results have further demonstrated that halide SSEs are quite promising owing to their wide electrochemical windows, good electrode stability, high humidity tolerance, and simple production processes. Halide SSEs and their application in ASSLBs are relentlessly advancing. These new developments make it necessary to revisit halide SSEs for potential applications in ASSLBs. Among halide SSEs, Li_3MX_6 (M = Sc, Y, Ho, Er, X = Cl, Br)-type SSEs have received wide attention. However, there is still a large gap between their experimental and theoretical results. To date, only a few halide SSEs, such as Li_3YBr_6 and Li_3InCl_6, have achieved a high ionic conductivity over 10^{-3} S cm^{-1} at RT. In addition, chloride-based SSEs showed an oxidation onset voltage of approximately 4 V, which cannot fully meet the electrolyte needs of high-voltage cathodes. Therefore, a tremendous amount of work is urgently required to improve ionic conductivity and optimize the electrochemical stability window in chloride-based SSEs.

The Li_3YBr_6, Li_3InCl_6, and Li_3InBr_6 SSEs, which possess a cubic close-packed (ccp)-like anion arrangement, display

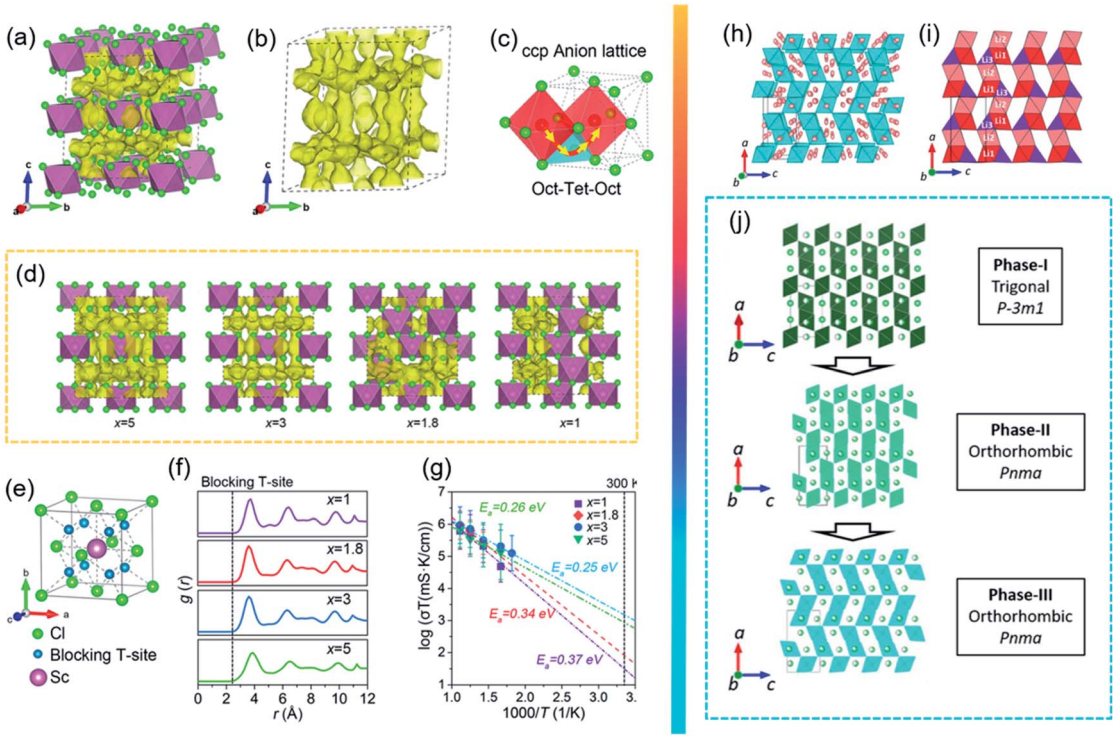

Fig. 10 (a and b) The Li^+ probability density based on AIMD simulations. (c) The Li^+ migration pathways of the Li_3ScCl_6 structure. (d) The Li^+ probability density marked by yellow isosurfaces of Li_5ScCl_8 ($x = 5$), Li_3ScCl_6 ($x = 3$), $Li_{1.8}ScCl_{4.8}$ ($x = 1.8$) and $LiScCl_4$ ($x = 1$) structures along the *a* axis. (e) The blocking effect of Sc. (f) Radial distribution function (rdf) of Sc–Li ions in the Li_xScCl_{3+x} ($x = 1$, 1.8, 3, and 5) SSEs. (g) Arrhenius plot of Li^+ diffusivity in Li_xScCl_{3+x} ($x = 1$, 1.8, 3, and 5) from AIMD simulations. Reproduced from ref. 167 with permission from the American Chemical Society, copyright 2020. (h) The crystal structure of $Li_{2.5}Er_{0.5}Zr_{0.5}Cl$. (i) Li connectivity along the [100] direction. (j) Phase evolution of $Li_3M_{1-x}Zr_xCl_6$ (M = Er, Y) upon Zr substitution. Reproduced from ref. 164 with permission from the American Chemical Society, copyright 2020.

relatively high ionic conductivities of 1–2 × 10^{-3} S cm.[67,68,164,166] Furthermore, theoretical calculations demonstrated that halide SSEs with ccp anion sublattices could display high ionic conductivities.[167] Inspired by the possibility of achieving fast Li^+ migration in ccp halide SSEs, new routes have opened in the development of ASSLBs. Recently, Li_xScCl_{3+x} SSEs (x = 2.5, 3, 3.5, and 4) were synthesized by a simple co-melting strategy from LiCl and $ScCl_3$. The structural evolution and ionic diffusion mechanisms in Li_xScCl_{3+x} were also systematically explored, and it was found that the vacancy concentration has the opposite trend with increasing x in Li_xScCl_{3+x} (Fig. 10). The Li^+ probability density and migration pathways were fitted based on AIMD simulations (Fig. 10a–c). The site occupations of metal/vacancies favoured Li^+ migration within the local structure (Fig. 10e–g). As a result, the obtained Li_3ScCl_6 showed a high ionic conductivity of 3 × 10^{-3} S cm^{-1}. Moreover, the all-solid-state $LiCoO_2$/Li_3ScCl_6/In full cell exhibited a long cycle life and a wide electrochemical window of 0.9–4.3 V. Note that Li_3ScCl_6 was not stable towards Li in the initial cycles of plating/stripping.[168] To enhance the ionic conductivity, the covalent substitution of metal ions was also an effective strategy to introduce vacancies in the mobile ion sublattice. Nazar *et al.* prepared a class of mixed-metal chloride solid-state electrolytes, $Li_{3-x}M_{1-x}Zr_xCl_6$ (M = Y, Er) SSEs. These new halide SSEs exhibited high ionic conductivities (up to 1.4 mS cm^{-1} at RT) due to their unique new structures (Fig. 10h and i). In Fig. 10j, combining neutron and single-crystal X-ray diffraction methods, the evolution of new structures after a Zr substitution revealed trigonal to orthorhombic phase transition processes. Most importantly, chloride SSEs without any protective coating showed excellent oxidation stability. When using unprotected $LiCoO_2$ as the cathode material, ASSLBs exhibited exceptional electrochemical oxidation stability up to 4.5 V at RT.[165]

Remarkably, halide SSEs based on close-packed anion arrangements or covalent substitution of metal ions exhibited a high ionic conductivity. However, the chemical and electrochemical stability was difficult to satisfy with both high oxidation and low reduction voltages in full battery applications. One of the possible solutions is to combine halide SSEs and other SSEs to be compatible with cathode and anode materials, respectively. Unlike chloride SSEs, fluoride SSEs exhibit a wide electrochemical stability window (~6 V). However, they have the lowest ionic conductivity among halide SSEs. To solve this problem, tuning the chemical composition of lithium difluoro(oxalato)borate (LiDFOB) and PEO can heighten the stability and improve the ionic conductivity in CSSEs,[169,170] which undoubtedly proves the possibility of modifying CSSEs with other types of SSEs. Therefore, the lower performance compared to other SSEs can be enhanced by various physical approaches and chemical strategies. It is predicted that halide SSEs will become more deserving of in-depth attention, and their commercialization in ASSLBs will be realized in the near future.

Table 1 List of representative composite solid-state electrolytes and their properties

	CSSEs	Conductivity (S cm^{-1})	Characteristics	Stability *vs.* Li/Li^+ (V)	Cycle performance	Ref.
Polymer-based	PEO/GDC/LSGM	10^{-4}, 30 °C	Reduced interfacial resistance	4.8	100 cycles (Li‖CSSE‖NMC)	93
	PEO/LLZO	1.1 × 10^{-4}, 40 °C	Reduced interfacial resistance	>4	200 cycles (Li‖CSSE‖S)	94
	PVDF–PVAC	4.8 × 10^{-4}, RT	Good flexibility	4.8	200 cycles (Li‖CSSE‖LCO)	101
	PEO/PEG–LGPS	9.83 × 10^{-4}, RT	Good interfacial compatibility	5.1	Over 3200 h (Li‖CSSE‖Li)	103
	PCE/LGPS/PCE	2.12 × 10^{-3}, RT	Good thermal stability	4.1	120 cycles (Li‖CSSE‖LFP)	106
Oxide-based	PEO/LLZTO	10^{-4}, 55 °C	High mechanical strength	5.0	100 cycles (Li‖CSSE‖LFP)	56
	Sandwich-PEO/LLZTO	9.1 × 10^{-5}, 55 °C	Freestanding and flexible, 11.3 MPa	5.03	200 cycles (Li‖CSSE‖LFP)	114
	LAGP–PEO	1.3 × 10^{-3}, 60 °C	High thermal stability	4.5	300 cycles (Li‖CSSE‖LFP)	116
	Vertically aligned LAGP–PEO	1.11 × 10^{-3}, 60 °C	Good interfacial compatibility	4.5	300 cycles (Li‖CSSE‖LFP)	117
Hydride-based	$Li_4(BH_4)_3I$@SBA-15	2.5 × 10^{-4}, 35 °C	Good interfacial contact	5.0	350 h (Li‖CSSE‖Li)	135
	$90LiBH_4$:$10P_2S_5$	10^{-3}, 27 °C	Good interfacial contact	5.0	10 cycles (LiIn‖CPE‖TiS_2)	138
	$0.7Li(CB_9H_{10})$–$0.3Li(CB_{11}H_{12})$	6.7 × 10^{-3}, 25 °C	High stability and flexible	5.0	300 h (Li‖CSSE‖Li)	84
	$Li(NH_3)_nBH_4$ ($0 < n \leq 2$)	2.21 × 10^{-3}, 40 °C	Good interfacial contact	>3.7	12 h (Li‖CSSE‖Li)	76
Sulfide-based	$Li_{9.54}Si_{1.74}P_{1.44}S_{11.7}Cl_{0.3}$	2.5 × 10^{-2}	Good interfacial contact	2.6	1000 cycles (LTO‖CSSE‖LCO)	10
	$78Li_2S$–$22P_2S_5$/polymer	4–7 × 10^{-4}, RT	Self-standing	3.0	100 cycles (LiIn‖CPE‖S–CNT)	58
	LPS/LLZO	5.36 × 10^{-4}, 25 °C	Good interfacial stability and contact	5.0	4500 min (Li‖CSSE‖Li)	158
	LPS–LiBH4	1.6 × 10^{-3}, RT	Good interfacial contact	5.0	5 cycles (Li‖CSSE‖TiS_2)	159
Halide-based	Li_xScCl_{3+x}	3 × 10^{-3}, RT	Good interfacial stability	4.3	160 cycles (Li‖CSSE‖LCO)	168
	$Li_{3-x}M_{1-x}Zr_xCl_6$ (M = Y, Er)	1.4 × 10^{-3}, RT	Good interfacial stability	4.5	200 cycles ($Li_{11}Sn_6$‖CSSE‖LCO)	165
	Li_3ErCl_6	3.15 × 10^{-4}, RT	Good oxidative stability	—	—	163
	PEO/LiDFOB–40wt% EMImTFSI	1.85 × 10^{-4}, 30 °C	Good interfacial contact	4.0	50 cycles (Li‖CSSE‖LFP)	170

Mobile ion migration mechanism in CSSEs

A comprehensive summary of different CSSEs, including polymer-based, oxide-based, hydride-based, sulfide-based and halide-based CSSEs, is provided in Table 1. For practical application in ASSBs, in addition to the ionic conductivity, electrochemical stability window, chemical compatibility, and mechanical properties, other properties such as thermal stability, fabrication processes, cost, device integration and environmental friendliness are also important.[11,171,172] In 2017, Manthiram *et al.* summarized the properties of the existing solid electrolyte materials and visualized those properties in radar plots.[11] It is clear that single solid-state electrolytes have difficulties satisfying the increasing demands in our daily life. Even though significant progress has been achieved, huge challenges still remained for CSSEs to seek an equilibrium relationship, which minimizes the weaknesses of individual SSEs to enhance the overall performance. Therefore, it is important to summarize previous achievements in order to understand, design, and fabricate novel CSSEs. Fig. 11 briefly describes the migration mechanism of lithium ions in different kinds of composite solid-state electrolytes. For polymer-based electrolytes, the diffusion in the polymeric host is based on ether linkages. However, with the increase of inorganic fillers, the ion transport gradually transits to the newly formed interphase between the dispersed crystalline and polymer matrix (Fig. 11a).[173] It is noticed that many solid-state electrolytes turn out to be superionic phases only at high temperature, such as hydride-based electrolytes (Fig. 2b).[173] Typical approaches, including cationic/anionic doping and compositing, could provide an effective method to stabilize the metastable phase *via* interfacial interactions. Recent studies have suggested that the ion transport of sulfide- and halide-based SSEs strongly depends on the ion channels formed by the special crystal structure.[174] For instance, the transformation of Li_3PS_4 from the glassy state to the crystalline state after heat treatment can effectively improve its ionic conductivity (Fig. 11c–f). In this case, understanding the basic conduction mechanism helps design better composite SSEs. In this section, we discuss how to

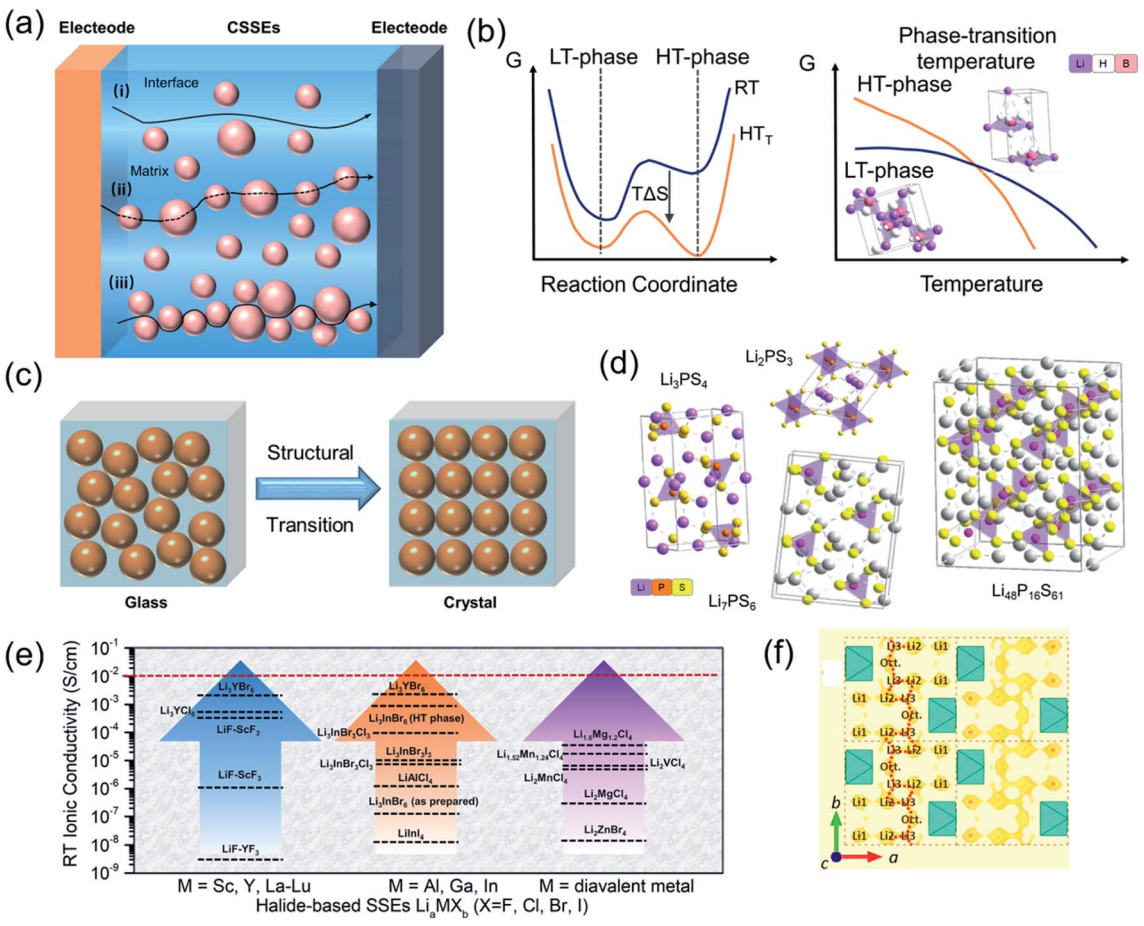

Fig. 11 (a) Illustration of ion conduction paths in polymer-based CSSEs and inorganic material-based CSSEs. (b) Free energy diagram of crystalline SSEs with a phase transition. (c and d) Structural transition and common sulfide crystal structures. Reproduced from ref. 173 with permission from the Royal Society of Chemistry, copyright 2020. (e) Summary of the reported RT ionic conductivities of representative halide SSEs. Reproduced from ref. 174 with permission from the Royal Society of Chemistry, copyright 2020. (f) 1D migration pathway of the crystal structure of $Li_{2.5}Er_{0.5}Zr_{0.5}Cl$ in the *ab* plane. Reproduced from ref. 165 with permission from the American Chemical Society, copyright 2020.

combine hosts with dispersed phases to make an ideal solid-state electrolyte with high ionic conductivities and favourable electrochemical stability.

By combining isotope labelling and solid-state Li NMR to track the ion-diffusion pathway, Hu *et al.* first provided experimental evidence to show that Li ions favour the pathway through the LLZO ceramic phase, not the interface or the PEO polymer phase.[175] After that, Pan *et al.* prepared a flexible composite solid electrolyte membrane consisting of inorganic solid particles $Li_{1.3}Al_{0.3}Ti_{1.7}(PO_4)_3$ (LATP), PEO, and boronized polyethylene glycol (BPEG), which provided good mechanical strength and physically inhibited the free growth of lithium dendrites. The authors discussed the relationships between the stability against lithium dendrite formation and the combination of well-designed components. As proposed in Fig. 12a, the growth of lithium dendrites could easily penetrate the SPE membrane, while the close packing of the inorganic particles worked as a physical barrier to restrict the free growth of lithium dendrites in the CSE membrane. The post-cycling SEM images of the Li-electrolyte interfaces in Fig. 12b–d showed that CSE-B-71515 (LATP, PEO and BPEG in the weight ratio of 70 : 15 : 15) had the smoothest Li surface and Fig. 12e showed that CSE-B-71515 had the smallest impedance value. The main reason was the effect of BPEG on lithium dendrite formation in Fig. 12f. The addition of BPEG oligomers disorganized the crystallinity of the PEO domain and improved ionic conductivity. Additionally, the planar structure of the oligomers chemically enabled homogeneous lithium plating/stripping on the lithium metal and reduced the polarization effects.[176]

However, the mechanism of dendrite formation and propagation remains unclear. Uneven Li^+ transport across the electrode–electrolyte interface causes heterogeneous nucleation, which is tied to dendrite formation during electrodeposition. To solve the safety problem induced by lithium dendrites, high shear modulus (G_s) CSSEs have been prioritized. In this case, the mechanism associated with dendrite formation can be modelled using Butler–Volmer physics:[177]

$$\frac{i_{\text{deformed}}}{i_{\text{undeformed}}} = \exp\left(\frac{(1-\alpha_a)\Delta\mu_{e^-}}{RT}\right)^2$$

where i is the current density at either a deformed or undeformed interface, α_a is the anodic charge-transfer coefficient, and $\Delta\mu_{e^-}$ is the change in electrochemical potential of the electron at a deformed interface. In this equation, the mechanical stresses and interfacial surface tension are the only factors for potential chemical changes. For stable electrodeposition, it needs to be ensured that i_{deformed} has a lower value than $i_{\text{undeformed}}$ at the peaks and a higher value in the valleys. Thus, $\Delta\mu_{e^-}$ should be negative.[177–179] In addition, γ is negligible, and the deviatoric stress is always destabilizing. Therefore, $\Delta\mu_{e^-}$

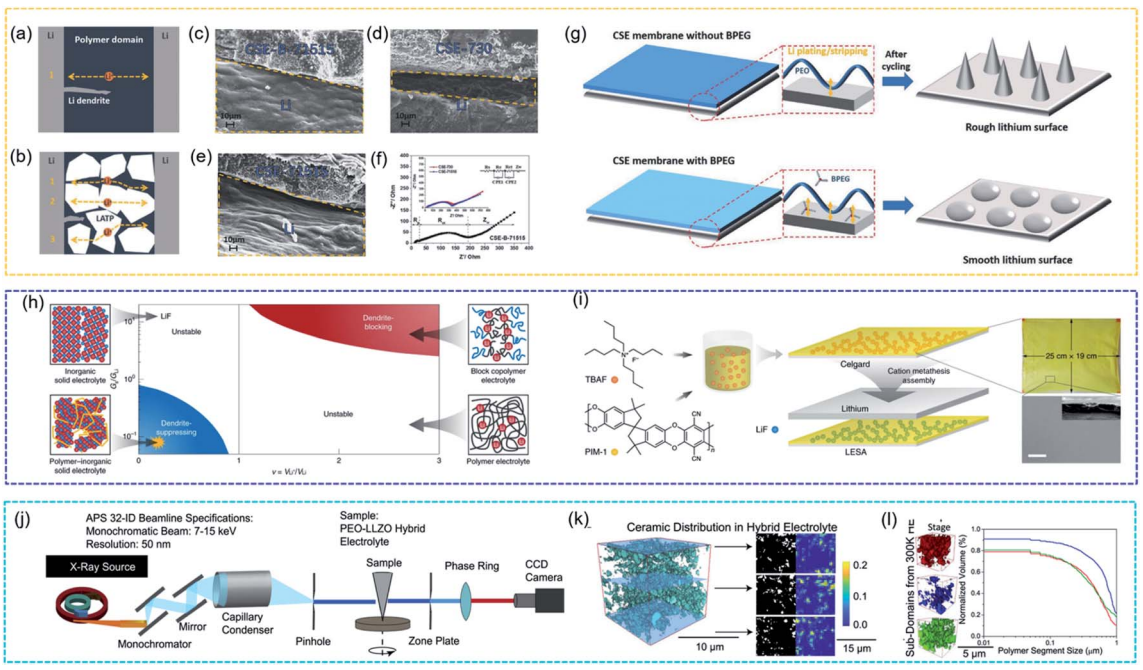

Fig. 12 Proposed lithium ion transfer pathways and lithium dendrite growth in SSEs (a) without inorganic particles and (b) with closely packed inorganic particles. (c–e) SEM images of the Li/CSE membrane interface in symmetrical cells after cycling, and corresponding to (f) electrochemical impedance spectra. (g) Schematic showing lithium plating/stripping processes with different CSE membranes. Reproduced from ref. 175 with permission from Wiley-VCH, copyright 2017. (h) Chemomechanical model underlying the successes and failures of SSEs during charging. (i) Schematic figure of prepared nano-LiF@PIM CSSEs. Scale bar, 1 μm. Reproduced from ref. 181 with permission from Nature Publishing Group, copyright 2020. (j) Schematic diagram of synchrotron nano-tomography characterization through the transmission X-ray microscopy technique. (k) Representative volume showing the ceramic and the polymer phase distribution within the CSSE. (l) Representative ceramic substructures and the polymer size distribution of the CSSE. Reproduced from ref. 186 with permission from Elsevier Inc., copyright 2020.

is dominated by the hydrostatic stress term, which is a function of V_{Li^+}, V_{Li}, G_s and G_{Li}. Hence, Helms *et al.* built a chemo-mechanical model (Fig. 12h) underlying the successes and failures of SSEs in stabilizing Li metal anodes according to the volume ratio $\upsilon = V_{Li^+}/V_{Li}$. For $\upsilon > 1$, $\Delta\mu_{e^-}$ becomes negative only when SSEs with $G_s/G_{Li} > 2.2$ are needed to block dendrite propagation.[180] Then, when $G_s/G_{Li} < 0.7$ and $\upsilon < 1$, density-driven suppression of dendrites is achievable with low volume changes of the soft SSEs. However, polymer electrolytes, known as soft electrolytes, generally undergo large volume expansion because the formed solvation 'cages' of Li^+ result in $\upsilon > 1$. To confirm their predicted dendrite-suppressing character in ASSBs, Helms *et al.* successfully prepared nano-LiF@PIM CSSEs using an *in situ* cation metathesis (Fig. 12i).[181] The redesigned CSSEs showed minimally reconfigurable, ceramic-like, ion-conducting domains, which were embedded in a soft, polymer-like matrix with a relatively low shear modulus. Specifically, LiF@PIM composites were useful for Li–S and Li–NMC-622 cells, which exhibited superior performance, suggesting a path forward for dendrite suppression.

CSSEs contain numerous solid/solid interfaces, including intrinsic and extrinsic interfaces, the former one is the contact region between the matrix phase and mixed media phase, and the later one is the contact surface between the electrode and electrolyte. These interfaces are responsible for ion-transportation, electrode/electrolyte compatibility, and stability in solid-state batteries. Understanding and evaluating interfacial properties have a significant effect on the rational design of ASSBs. Currently, there are few studies that report the effect of extrinsic interfaces on electrochemical performance. Extrinsic interfaces are responsible for high interfacial resistances, which can cause a catastrophic failure in capacity due to Li dendrites,[182,183] dead Li,[184] or interfacial delamination.[185]

Hatzell's group systematically evaluated the relationship between the electrolyte structure and extrinsic interfaces in solid-state batteries and investigated how extrinsic interfaces impacted electrochemical performance in ASSBs. By design, CSSEs with similar transport properties were manufactured and displayed varying interfacial properties. The mechanical, adhesion, and interfacial ion-transport properties in the extrinsic interfaces were estimated using an effective mean field theory model and atomic force microscopy techniques (AFM). They found that the difference in physical properties at the extrinsic interfaces depended on the distribution of inorganic particles in CSSEs. Hence, synchrotron X-ray nanotomography was performed to evaluate the heterogeneous distribution of inorganic materials. Then, combined with physics-based modelling, the 3D-structure of CSSEs was reconstructed to elucidate the origin of heterogeneous interfacial properties. These findings revealed that mechanical properties, rather than transport properties at the extrinsic interface, largely dictated the electrochemical performance. To achieve facile and long-life ASSBs, microstructural control over inorganic constituents may provide a pathway towards tailoring interfacial properties with spatial control, which can be achieved by controlling the CSSE nano- and microstructures (Fig. 12j and k).[186] Despite the significant achievements in state-of-the-art CSSEs, the above detailed mechanistic study is insufficient to form a complete system to support the advanced performance of CSSEs and realize their application in ASSBs.

Summary and outlook

All solid-state batteries have experienced rapid progress and have drawn increasing attention owing to the introduction of high-energy density metal anodes. Developing advanced CSSEs is considered to be one of the most promising directions to achieve a breakthrough in solid-state battery technology. With more and more attempts, various hosts and dispersed phases are combined into potential CSSEs, which not only have high ionic conductivity, but also show good stability and properties. For instance, composites consisting of "oxides and polymers" are flexible and mechanically robust. A new strategy of forming a thin electrolyte is introduced by creating sulfide-in-polymer composites. Hydride-based CSSEs have good stability against metallic Li, which help overcome the side reaction problem of sulfides/oxides. Meanwhile, sulfide/oxide-based CSSEs also match high-voltage cathode materials. Although SSEs have been widely believed to be safer for ASSB application, such a point of view still lacks sufficient data support, in particular for batteries with Li as an anode electrode. Challenges including continuous interfacial side reactions, limited electrochemical window, poor air stability, large volume expansion/shrinkage, undesirable dendrite growth, inescapable heat generation and thermal runaway should be conquered for achieving better performance.[187] For example, very recent progress suggests that the release of oxygen from SSEs at increased temperatures is found to be responsible for thermal runaway with Li. It is also demonstrated that oxide SSEs exhibit different thermal stability against highly reactive metallic Li.[188] A further artificial layer (such as Al_2O_3, Li_2CO_3) can help stabilize the interface between Li and SSEs. For example, solid/solid interfacial architecturing through atomic layer deposition of Al_2O_3 on the SPE surface could suppress the "shuttle effect" of lithium polysulfide intermediates in the SPE and increase the interfacial compatibility between the metal lithium anode and the SPE.[189] Considering the unique advantages of SSEs, some perspectives presented herein are based on CSSEs.

Lithium dendrite growth is mostly discovered in single polymers or inorganic electrolytes based on recent research contributions. Among CSSEs, there are few reports on the growth of lithium dendrites, which is an open field for further research. Information on architecture and composite content, component contribution and ion-conduction tunnels, along with lithium deposition behaviour is required for the design of advanced CSSEs.

Currently, most syntheses of CSSEs are based on dissolving particles in a matrix, or compounding layer by layer. The interfacial contacts between two phases and the ion transport mechanism need further investigation. More importantly, advanced CSSEs need to be designed from nanoscale. Therefore, it also requires *in situ*/*operando* characterization techniques, such as time-of-flight secondary-ion mass spectrometry and *in situ* electrochemical spherical aberration electron

microscopy, to provide an in-depth study on the interfacial dynamics and ion transport mechanism.

To further improve the capacity and energy density of CSSE based ASSBs, matching suitable and smart cathode materials according to the electrochemical window and stability is another key objective. This could be realized through increasing more sites for active substances by constructing efficient electronic and ionic conductive networks. The interfacial design between the cathode and anode would progress from micron to nanoscale, and the mechanism of ion transport would transit from interfacial contact into atomic contact, which may rely on advanced nanotechnology.

From traditional single SSEs to composite SSEs is a research trend that we believe. Many issues have been exposed along with thorough studies, but fortunately the pace has never stopped to face challenges. Fully exploiting their potential has high scientific and practical value for large-scale energy storage in ASSBs in the near future.

Abbreviations

AFM	Atomic force microscopy
ASR	Area-specific resistance
ASSLBs	All-solid-state lithium batteries
BPEG	Boronized polyethylene glycol
CEI	Cathode electrolyte interphase
CPEs	Composite polymer electrolytes
CPSE	Ceramic/polymer solid-state electrolyte
CSSEs	Composite solid-state electrolytes
DFT	Density functional theory
DSC	Differential scanning calorimeter
GDC	$Gd_{0.1}Ce_{0.9}O_{1.9}5$
GO	Graphene oxide
G_s	Shear modulus
LAGP	$Li_{1.5}Al_{0.5}Ge_{1.5}(PO_4)_3$
LATP[99]:	$Li_{1.4}Al_{0.4}Ti_{1.6}(PO_4)_3$
LATP[176]:	$Li_{1.3}Al_{0.3}Ti_{1.7}(PO_4)_3$
LBO	Li_3BO_3
LCO	$LiCoO_2$
LFP	$LiFePO_4$
LGPS	$Li_{10}GeP_2S_{12}$
LIBs	Lithium-ion batteries
LIPON	Lithium phosphorus oxynitride
LLTO	$Li_{0.33}La_{0.557}TiO_3$
LLZO	$Li_7La_3Zr_2O_{12}$
LLZTO[56,91,100]	$Li_{6.4}La_3Zr_{1.4}Ta_{0.6}O_{12}$
LLZTO[126]	$Li_{6.75}La_3Zr_{1.75}Ta_{0.25}O_{12}$
LSGM	$La_{0.8}Sr_{0.2}Ga_{0.8}Mg_{0.2}O_{2.55}$
LSTZ	$Li_{3/8}Sr_{7/16}Ta_{3/4}Zr_{1/4}O_3$
NASICON	Sodium superionic conductor
Ni-MH	Nickel-metal hydride
NMR	Nuclear magnetic resonance
PAN	Polyacrylonitrile
PEG	Polyethylene glycol
PEGDME	Poly-(ethylene glycol)-dimethyl ether
PEO	Polyethylene oxide
PMMA	Polymethyl methacrylate
PPO–PEO–PPO	Hydrophobic–hydrophilic–hydrophobic triblock copolymers
PVAC	Polyvinyl acetate
PVDF	Polyvinylidene fluoride
RT	Room temperature
SEI	Solid electrolyte interphase
SIEs	Solid inorganic electrolytes
SPEs	Solid polymer electrolytes
SS	Stainless steel
SSE(s)	Solid-state electrolyte(s)
ASSLSBs	All-solid-state Li–S batteries
Thio-LISICON	Thio-lithium superionic conductor
TMS	Tetramethylene sulfone

Conflicts of interest

There are no conflicts to declare.

Acknowledgements

This work was supported by "the Fundamental Research Funds for the Central Universities, No. NS2020039, Open Fund of Key Laboratory of Materials Preparation and Protection for Harsh Environment (Nanjing University of Aeronautics and Astronautics), and Ministry of Industry and Information Technology No. XCA20013-2. T. Z., W. Z. and X. Y. acknowledge support from the National Natural Science Foundation of China (51625102, 51802154 and 51903047). W. Z. acknowledges support from the Natural Science Foundation of Jiangsu Province (grant BK20180407). X. Y. acknowledges support from the Open Fund of Jiangsu Key Laboratory of Electrochemical Energy Storage Technologies No. EEST2019-2. W. H. acknowledges support from the Postgraduate Research & Practice Innovation Program of Jiangsu Province (KYCX20_0192).

Notes and references

1 B. Dunn, H. Kamath and J. M. Tarascon, *Science*, 2011, **334**, 928–935.
2 J.-M. Tarascon and M. Armand, *Nature*, 2001, **414**, 359–367.
3 J. B. Goodenough and K. S. Park, *J. Am. Chem. Soc.*, 2013, **135**, 1167–1176.
4 I. H. Son, J. Hwan Park, S. Kwon, S. Park, M. H. Rümmeli, A. Bachmatiuk, H. J. Song, J. Ku, J. W. Choi, J. Choi, S.-G. Doo and H. Chang, *Nat. Commun.*, 2015, **6**, 7393.
5 Q. Pang, X. Liang, C. Y. Kwok and L. F. Nazar, *Nat. Energy*, 2016, **1**, 16132.
6 B. Anasori, M. R. Lukatskaya and Y. Gogotsi, *Nat. Rev. Mater.*, 2017, **2**, 16098.
7 J. Wan, J. Xie, X. Kong, Z. Liu, K. Liu, F. Shi, A. Pei, H. Chen, W. Chen, J. Chen, X. Zhang, L. Zong, J. Wang, L. Q. Chen, J. Qin and Y. Cui, *Nat. Nanotechnol.*, 2019, **14**, 705–711.
8 Y. Wang, W. D. Richards, S. P. Ong, L. J. Miara, J. C. Kim, Y. Mo and G. Ceder, *Nat. Mater.*, 2015, **14**, 1026–1031.

9 A. Miura, N. C. Rosero-Navarro, A. Sakuda, K. Tadanaga, N. H. H. Phuc, A. Matsuda, N. Machida, A. Hayashi and M. Tatsumisago, *Nat. Rev. Chem.*, 2019, **3**, 189–198.
10 Y. Kato, S. Hori, T. Saito, K. Suzuki, M. Hirayama, A. Mitsui, M. Yonemura, H. Iba and R. Kanno, *Nat. Energy*, 2016, **1**, 16030.
11 A. Manthiram, X. Yu and S. Wang, *Nat. Rev. Mater.*, 2017, **2**, 16103.
12 Y. Oumellal, A. Rougier, G. A. Nazri, J.-M. Tarascon and L. Aymard, *Nat. Mater.*, 2008, **7**, 916–921.
13 J. Janek and W. G. Zeier, *Nat. Energy*, 2016, **1**, 1–4.
14 J. K. Nørskov, T. Bligaard, J. Rossmeisl and C. H. Christensen, *Nat. Chem.*, 2009, **1**, 37–46.
15 X. Han, Y. Gong, K. Fu, X. He, G. T. Hitz, J. Dai, A. Pearse, B. Liu, H. Wang, G. Rubloff, Y. Mo, V. Thangadurai, E. D. Wachsman and L. Hu, *Nat. Mater.*, 2017, **16**, 572–579.
16 N. Kamaya, K. Homma, Y. Yamakawa, M. Hirayama, R. Kanno, M. Yonemura, T. Kamiyama, Y. Kato, S. Hama, K. Kawamoto and A. Mitsui, *Nat. Mater.*, 2011, **10**, 682–686.
17 Z. Lin, Z. Liu, N. J. Dudney and C. Liang, *ACS Nano*, 2013, **7**, 2829–2833.
18 E. Rangasamy, Z. Liu, M. Gobet, K. Pilar, G. Sahu, W. Zhou, H. Wu, S. Greenbaum and C. Liang, *J. Am. Chem. Soc.*, 2015, **137**, 1384–1387.
19 W. S. Tang, M. Matsuo, H. Wu, V. Stavila, W. Zhou, A. A. Talin, A. V. Soloninin, R. V. Skoryunov, O. A. Babanova, A. V. Skripov, A. Unemoto, S.-I. Orimo and T. J. Udovic, *Adv. Energy Mater.*, 2016, **6**, 1502237.
20 X. Wang, R. Xiao, H. Li and L. Chen, *Phys. Rev. Lett.*, 2017, **118**, 195901.
21 S. J. Sedlmaier, S. Indris, C. Dietrich, M. Yavuz, C. Dräger, F. Von Seggern, H. Sommer and J. Janek, *Chem. Mater.*, 2017, **29**, 1830–1835.
22 H. Yamane, M. Shibata, Y. Shimane, T. Junke, Y. Seino, S. Adams, K. Minami, A. Hayashi and M. Tatsumisago, *Solid State Ionics*, 2007, **178**, 1163–1167.
23 K. H. Park, Q. Bai, D. H. Kim, D. Y. Oh, Y. Zhu, Y. Mo and Y. S. Jung, *Adv. Energy Mater.*, 2018, **8**, 1800035.
24 Y. Meesala, A. Jena, H. Chang and R. S. Liu, *ACS Energy Lett.*, 2017, **2**, 2734–2751.
25 Z. Zhang, Y. Shao, B. Lotsch, Y. S. Hu, H. Li, J. Janek, L. F. Nazar, C. W. Nan, J. Maier, M. Armand and L. Chen, *Energy Environ. Sci.*, 2018, **11**, 1945–1976.
26 X. B. Cheng, R. Zhang, C. Z. Zhao and Q. Zhang, *Chem. Rev.*, 2017, **117**, 10403–10473.
27 F. Han, J. Yue, C. Chen, N. Zhao, X. Fan, Z. Ma, T. Gao, F. Wang, X. Guo and C. Wang, *Joule*, 2018, **2**, 497–508.
28 H. Liu, X. B. Cheng, J. Q. Huang, H. Yuan, Y. Lu, C. Yan, G. L. Zhu, R. Xu, C. Z. Zhao, L. P. Hou, C. He, S. Kaskel and Q. Zhang, *ACS Energy Lett.*, 2020, **5**, 833–843.
29 Y. Zhu, X. He and Y. Mo, *J. Mater. Chem. A*, 2016, **4**, 3253–3266.
30 B. Zhang, Z. Lin, L. W. Wang and F. Pan, *ACS Appl. Mater. Interfaces*, 2020, **12**, 6007–6014.
31 Y. Gao, Z. Yan, J. L. Gray, X. He, D. Wang, T. Chen, Q. Huang, Y. C. Li, H. Wang, S. H. Kim, T. E. Mallouk and D. Wang, *Nat. Mater.*, 2019, **18**, 384–389.
32 S. Wenzel, D. A. Weber, T. Leichtweiss, M. R. Busche, J. Sann and J. Janek, *Solid State Ionics*, 2016, **286**, 24–33.
33 H. Zhong, L. Sang, F. Ding, J. Song and Y. Mai, *Electrochim. Acta*, 2018, **277**, 268–275.
34 Y. Zhu, X. He and Y. Mo, *ACS Appl. Mater. Interfaces*, 2015, **7**, 23685–23693.
35 Z. Hou, J. Zhang, W. Wang, Q. Chen, B. Li and C. Li, *J. Energy Chem.*, 2020, **45**, 7–17.
36 A. Manthiram, *ACS Cent. Sci.*, 2017, **3**, 1063–1069.
37 D. E. Fenton, J. M. Parker and P. V. Wright, *Polymer*, 1973, **14**, 589.
38 R. Xue, H. Huang, L. Chen and K. Wang, *Solid State Ionics*, 1993, **59**, 1–4.
39 G. Dautzenberg, F. Croce, S. Passerini and B. Scrosati, *Chem. Mater.*, 1994, **6**, 538–542.
40 O. Bohnke, G. Frand, M. Rezrazi, C. Rousselot and C. Truche, *Solid State Ionics*, 1993, **66**, 97–104.
41 O. Bohnke, G. Frand, M. Rezrazi, C. Rousselot and C. Truche, *Solid State Ionics*, 1993, **66**, 105–112.
42 Y. Saito, H. Kataoka, E. Quartarone and P. Mustarelli, *J. Phys. Chem. B*, 2002, **106**, 7200–7204.
43 V. Arcella, A. Sanguineti, E. Quartarone and P. Mustarelli, *J. Power Sources*, 1999, **81–82**, 790–794.
44 X. Yu, *J. Electrochem. Soc.*, 1997, **144**, 524.
45 G. Y. Adachi, N. Imanaka and S. Tamura, *Chem. Rev.*, 2002, **102**, 2405–2429.
46 B. E. Francisco, C. R. Stoldt and J. C. M'Peko, *Chem. Mater.*, 2014, **26**, 4741–4749.
47 J. Płcharski and W. Weiczorek, *Solid State Ionics*, 1988, **28–30**, 979–982.
48 F. Zheng, M. Kotobuki, S. Song, M. O. Lai and L. Lu, *J. Power Sources*, 2018, **389**, 198–213.
49 X. Huang, C. Liu, Y. Lu, T. Xiu, J. Jin, M. E. Badding and Z. Wen, *J. Power Sources*, 2018, **382**, 190–197.
50 K. Fu, Y. Gong, B. Liu, Y. Zhu, S. Xu, Y. Yao, W. Luo, C. Wang, S. D. Lacey, J. Dai, Y. Chen, Y. Mo, E. Wachsman and L. Hu, *Sci. Adv.*, 2017, **3**, e1601659.
51 G. T. Hitz, D. W. McOwen, L. Zhang, Z. Ma, Z. Fu, Y. Wen, Y. Gong, J. Dai, T. R. Hamann, L. Hu and E. D. Wachsman, *Mater. Today*, 2019, **22**, 50–57.
52 N. Zhao, W. Khokhar, Z. Bi, C. Shi, X. Guo, L. Z. Fan and C. W. Nan, *Joule*, 2019, **3**, 1190–1199.
53 B. Liu, Y. Gong, K. Fu, X. Han, Y. Yao, G. Pastel, C. Yang, H. Xie, E. D. Wachsman and L. Hu, *ACS Appl. Mater. Interfaces*, 2017, **9**, 18809–18815.
54 R. Murugan, V. Thangadurai and W. Weppner, *Angew. Chem., Int. Ed.*, 2007, **46**, 7778–7781.
55 K. Fu, Y. Gong, T. Gregory Hitz, W. Dennis McOwen, Y. Li, S. Xu, Y. Wen, L. Zhang, C. Wang, G. Pastel, J. Dai, B. Liu, H. Xie, Y. Yao, E. D. Wachsman and L. Hu, *Energy Environ. Sci.*, 2017, **10**, 1568–1575.
56 L. Chen, Y. Li, S. P. Li, L. Z. Fan, C. W. Nan and J. B. Goodenough, *Nano Energy*, 2018, **46**, 176–184.
57 X. Li, X. Li, J. Liang, C. Wang, J. Luo, R. Li and X. Sun, *Energy Environ. Sci.*, 2018, **11**, 2828–2832.
58 Y. Zhang, R. Chen, S. Wang, T. Liu, B. Xu, X. Zhang, X. Wang, Y. Shen, Y. H. Lin, M. Li, L. Z. Fan, L. Li and C. W. Nan, *Energy Storage Mater.*, 2020, **25**, 145–153.

59 S. Chen, D. Xie, G. Liu, J. P. Mwizerwa, Q. Zhang, Y. Zhao, X. Xu and X. Yao, *Energy Storage Mater.*, 2018, **14**, 58–74.
60 H. D. Lim, X. Yue, X. Xing, V. Petrova, M. Gonzalez, H. Liu and P. Liu, *J. Mater. Chem. A*, 2018, **6**, 7370–7374.
61 H. Muramatsu, A. Hayashi, T. Ohtomo, S. Hama and M. Tatsumisago, *Solid State Ionics*, 2011, **182**, 116–119.
62 R. Xu, S. Zhang, X. Wang, Y. Xia, X. Xia, J. Wu, C. Gu and J. Tu, *Chem.–Eur. J.*, 2018, **24**, 6007–6018.
63 Q. Zhang, J. P. Mwizerwa, H. Wan, L. Cai, X. Xu and X. Yao, *J. Mater. Chem. A*, 2017, **5**, 23919–23925.
64 F. Han, J. Yue, X. Fan, T. Gao, C. Luo, Z. Ma, L. Suo and C. Wang, *Nano Lett.*, 2016, **16**, 4521–4527.
65 W. Weppner and R. A. Huggins, *Phys. Lett. A*, 1976, **58**, 245–248.
66 E. J. Plichta, *J. Electrochem. Soc.*, 1992, **139**, 1509.
67 Y. Tomita, A. Fuji-I, H. Ohki, K. Yamada and T. Okuda, *Chem. Lett.*, 1998, 223–224.
68 T. Asano, A. Sakai, S. Ouchi, M. Sakaida, A. Miyazaki and S. Hasegawa, *Adv. Mater.*, 2018, **30**, 1803075.
69 X. Li, J. Liang, N. Chen, J. Luo, K. R. Adair, C. Wang, M. N. Banis, T. Sham, L. Zhang, S. Zhao, S. Lu, H. Huang, R. Li and X. Sun, *Angew. Chem., Int. Ed.*, 2019, **131**, 16579–16584.
70 X. Li, J. Liang, J. Luo, M. Norouzi Banis, C. Wang, W. Li, S. Deng, C. Yu, F. Zhao, Y. Hu, T. K. Sham, L. Zhang, S. Zhao, S. Lu, H. Huang, R. Li, K. R. Adair and X. Sun, *Energy Environ. Sci.*, 2019, **12**, 2665–2671.
71 M. Matsuo and S. Orimo, *Adv. Energy Mater.*, 2011, **1**, 161–172.
72 D. Blanchard, A. Nale, D. Sveinbjörnsson, T. M. Eggenhuisen, M. H. W. Verkuijlen, Suwarno, T. Vegge, A. P. M. Kentgens and P. E. De Jongh, *Adv. Funct. Mater.*, 2015, **25**, 184–192.
73 M. Matsuo, Y. Nakamori, S. I. Orimo, H. Maekawa and H. Takamura, *Appl. Phys. Lett.*, 2007, **91**, 224103.
74 H. Maekawa, M. Matsuo, H. Takamura, M. Ando, Y. Noda, T. Karahashi and S. Orimo, *J. Am. Chem. Soc.*, 2009, **131**, 894–895.
75 P. López-Aranguren, N. Berti, A. H. Dao, J. Zhang, F. Cuevas, M. Latroche and C. Jordy, *J. Power Sources*, 2017, **357**, 56–60.
76 T. Zhang, Y. Wang, S. Isobe, N. Hashimoto, Y. Kojima, T. Song, H. Miyaoka, K. Shinzato, H. Miyaoka, T. Ichikawa, S. Shi and X. Zhang, *Joule*, 2018, **2**, 1522–1533.
77 H. T. T. Le, R. S. Kalubarme, D. T. Ngo, H. S. Jadhav and C. J. Park, *J. Mater. Chem. A*, 2015, **3**, 22421–22431.
78 C. Ma, K. Chen, C. Liang, C. W. Nan, R. Ishikawa, K. More and M. Chi, *Energy Environ. Sci.*, 2014, **7**, 1638–1642.
79 V. Thangadurai, H. Kaack and W. J. F. Weppner, *J. Am. Ceram. Soc.*, 2003, **86**, 437–440.
80 R. Murugan, V. Thangadurai and W. Weppner, *Angew. Chem., Int. Ed.*, 2007, **46**, 7778–7781.
81 S. Ramakumar, C. Deviannapoorani, L. Dhivya, L. S. Shankar and R. Murugan, *Prog. Mater. Sci.*, 2017, **88**, 325–411.
82 M. Murayama, R. Kanno, M. Irie, S. Ito, T. Hata, N. Sonoyama and Y. Kawamoto, *J. Solid State Chem.*, 2002, **168**, 140–148.
83 J. C. Bachman, S. Muy, A. Grimaud, H. H. Chang, N. Pour, S. F. Lux, O. Paschos, F. Maglia, S. Lupart, P. Lamp, L. Giordano and Y. Shao-Horn, *Chem. Rev.*, 2016, **116**, 140–162.
84 S. Kim, H. Oguchi, N. Toyama, T. Sato, S. Takagi, T. Otomo, D. Arunkumar, N. Kuwata, J. Kawamura and S. Orimo, *Nat. Commun.*, 2019, **10**, 1081.
85 Y. Aihara, S. Arai and K. Hayamizu, *Electrochim. Acta*, 2000, **45**, 1321–1326.
86 M. Faraday, *Philos. Trans. R. Soc. London*, 1833, **123**, 23–54.
87 M. Armand and J. M. Tarascon, *Nature*, 2008, **451**, 652–657.
88 About NAS Batteries|Products|NGK INSULATORS, LTD., https://www.ngk-insulators.com/en/product/nas/about/index.html, accessed 5 April 2020.
89 J. H. Choi, C. H. Lee, J. H. Yu, C. H. Doh and S. M. Lee, *J. Power Sources*, 2015, **274**, 458–463.
90 D. Lin, W. Liu, Y. Liu, H. R. Lee, P. C. Hsu, K. Liu and Y. Cui, *Nano Lett.*, 2016, **16**, 459–465.
91 S. H. S. Cheng, K. Q. He, Y. Liu, J. W. Zha, M. Kamruzzaman, R. L. W. Ma, Z. M. Dang, R. K. Y. Li and C. Y. Chung, *Electrochim. Acta*, 2017, **253**, 430–438.
92 H. Xu, P. H. Chien, J. Shi, Y. Li, N. Wu, Y. Liu, Y. Y. Hu and J. B. Goodenough, *Proc. Natl. Acad. Sci. U. S. A.*, 2019, **116**, 18815–18821.
93 A. N. Wu, P. H. Chien, Y. Qian, Y. Li, N. S. Grundish, B. Xu, H. Jin, Y. Y. Hu, G. Yu and J. B. Goodenough, *Angew. Chem., Int. Ed.*, 2020, **59**, 4131–4137.
94 X. Tao, Y. Liu, W. Liu, G. Zhou, J. Zhao, D. Lin, C. Zu, O. Sheng, W. Zhang, H. W. Lee and Y. Cui, *Nano Lett.*, 2017, **17**, 2967–2972.
95 P. Zhu, C. Yan, J. Zhu, J. Zang, Y. Li, H. Jia, X. Dong, Z. Du, C. Zhang, N. Wu, M. Dirican and X. Zhang, *Energy Storage Mater.*, 2019, **17**, 220–225.
96 S. Song, Y. Wu, W. Tang, F. Deng, J. Yao, Z. Liu, R. Hu, Alamusi, Z. Wen, L. Lu and N. Hu, *ACS Sustainable Chem. Eng.*, 2019, **7**, 7163–7170.
97 S. Tang, Q. Lan, L. Xu, J. Liang, P. Lou, C. Liu, L. Mai, Y. C. Cao and S. Cheng, *Nano Energy*, 2020, **71**, 104600.
98 J. N. Zhang, Q. Li, C. Ouyang, X. Yu, M. Ge, X. Huang, E. Hu, C. Ma, S. Li, R. Xiao, W. Yang, Y. Chu, Y. Liu, H. Yu, X. Q. Yang, X. Huang, L. Chen and H. Li, *Nat. Energy*, 2019, **4**, 594–603.
99 K. Nie, X. Wang, J. Qiu, Y. Wang, Q. Yang, J. Xu, X. Yu, H. Li, X. Huang and L. Chen, *ACS Energy Lett.*, 2020, **5**, 826–832.
100 J. H. Cha, P. N. Didwal, J. M. Kim, D. R. Chang and C. J. Park, *J. Membr. Sci.*, 2020, **595**, 117538.
101 X. Yu, L. Wang, J. Ma, X. Sun, X. Zhou and G. Cui, *Adv. Energy Mater.*, 2020, 1903939.
102 Y. Zhao, C. Wu, G. Peng, X. Chen, X. Yao, Y. Bai, F. Wu, S. Chen and X. Xu, *J. Power Sources*, 2016, **301**, 47–53.
103 K. Pan, L. Zhang, W. Qian, X. Wu, K. Dong, H. Zhang and S. Zhang, *Adv. Mater.*, 2020, 2000399.
104 J. Auvergniot, A. Cassel, D. Foix, V. Viallet, V. Seznec and R. Dedryvère, *Solid State Ionics*, 2017, **300**, 78–85.
105 J. Zhang, C. Zheng, J. Lou, Y. Xia, C. Liang, H. Huang, Y. Gan, X. Tao and W. Zhang, *J. Power Sources*, 2019, **412**, 78–85.

106 C. Wang, K. R. Adair, J. Liang, X. Li, Y. Sun, X. Li, J. Wang, Q. Sun, F. Zhao, X. Lin, R. Li, H. Huang, L. Zhang, R. Yang, S. Lu and X. Sun, *Adv. Funct. Mater.*, 2019, **29**, 1900392.
107 N. J. Dudney, J. B. Bates, R. A. Zuhr, C. F. Luck and J. D. Robertson, *Solid State Ionics*, 1992, **53–56**, 655–661.
108 H. Duan, Y. X. Yin, Y. Shi, P. F. Wang, X. D. Zhang, C. P. Yang, J. L. Shi, R. Wen, Y. G. Guo and L. J. Wan, *J. Am. Chem. Soc.*, 2018, **140**, 82–85.
109 M. Du, K. Liao, Q. Lu and Z. Shao, *Energy Environ. Sci.*, 2019, **12**, 1780–1804.
110 A. Jena, Y. Meesala, S. F. Hu, H. Chang and R. S. Liu, *ACS Energy Lett.*, 2018, **3**, 2775–2795.
111 Y. Shao, H. Wang, Z. Gong, D. Wang, B. Zheng, J. Zhu, Y. Lu, Y. S. Hu, X. Guo, H. Li, X. Huang, Y. Yang, C. W. Nan and L. Chen, *ACS Energy Lett.*, 2018, **3**, 1212–1218.
112 W. Feng, X. Dong, X. Zhang, Z. Lai, P. Li, C. Wang, Y. Wang and Y. Xia, *Angew. Chem., Int. Ed.*, 2020, **59**, 5346–5349.
113 C. Wang, Y. Yang, X. Liu, H. Zhong, H. Xu, Z. Xu, H. Shao and F. Ding, *ACS Appl. Mater. Interfaces*, 2017, **9**, 13694–13702.
114 H. Huo, Y. Chen, J. Luo, X. Yang, X. Guo and X. Sun, *Adv. Energy Mater.*, 2019, **9**, 1804004.
115 S. Kalnaus, A. S. Sabau, W. E. Tenhaeff, N. J. Dudney and C. Daniel, *J. Power Sources*, 2012, **201**, 280–287.
116 A. Li, X. Liao, H. Zhang, L. Shi, P. Wang, Q. Cheng, J. Borovilas, Z. Li, W. Huang, Z. Fu, M. Dontigny, K. Zaghib, K. Myers, X. Chuan, X. Chen and Y. Yang, *Adv. Mater.*, 2020, **32**, 1905517.
117 X. Wang, H. Zhai, B. Qie, Q. Cheng, A. Li, J. Borovilas, B. Xu, C. Shi, T. Jin, X. Liao, Y. Li, X. He, S. Du, Y. Fu, M. Dontigny, K. Zaghib and Y. Yang, *Nano Energy*, 2019, **60**, 205–212.
118 M. J. Palmer, S. Kalnaus, M. B. Dixit, A. S. Westover, K. B. Hatzell, N. J. Dudney and X. C. Chen, *Energy Storage Mater.*, 2020, **26**, 242–249.
119 M. Huang, T. Liu, Y. Deng, H. Geng, Y. Shen, Y. Lin and C. W. Nan, *Solid State Ionics*, 2011, **204–205**, 41–45.
120 K. Tadanaga, R. Takano, T. Ichinose, S. Mori, A. Hayashi and M. Tatsumisago, *Electrochem. Commun.*, 2013, **33**, 51–54.
121 R. Takano, K. Tadanaga, A. Hayashi and M. Tatsumisago, *Solid State Ionics*, 2014, **255**, 104–107.
122 N. C. Rosero-Navarro, T. Yamashita, A. Miura, M. Higuchi and K. Tadanaga, *Solid State Ionics*, 2016, **285**, 6–12.
123 R. H. Shin, S. I. Son, Y. S. Han, Y. Do Kim, H. T. Kim, S. S. Ryu and W. Pan, *Solid State Ionics*, 2017, **301**, 10–14.
124 M. H. Braga, N. S. Grundish, A. J. Murchison and J. B. Goodenough, *Energy Environ. Sci.*, 2017, **10**, 331–336.
125 X. Lü, J. W. Howard, A. Chen, J. Zhu, S. Li, G. Wu, P. Dowden, H. Xu, Y. Zhao and Q. Jia, *Adv. Sci.*, 2016, **3**, 1500359.
126 Y. Tian, F. Ding, H. Zhong, C. Liu, Y. B. He, J. Liu, X. Liu and Q. Xu, *Energy Storage Mater.*, 2018, **14**, 49–57.
127 R. Mohtadi and S. Orimo, *Nat. Rev. Mater.*, 2016, **2**, 16091.
128 S. Orimo, Y. Nakamori, J. R. Eliseo, A. Zu and C. M. Jensen, *Chem. Rev.*, 2007, **107**, 4111–4132.
129 A. Unemoto, T. Ikeshoji, S. Yasaku, M. Matsuo, V. Stavila, T. J. Udovic and S.-I. Orimo, *Chem. Mater.*, 2015, **27**, 5407–5416.
130 F. Mo, J. Ruan, S. Sun, Z. Lian, S. Yang, X. Yue, Y. Song, Y. Zhou, F. Fang, G. Sun, S. Peng and D. Sun, *Adv. Energy Mater.*, 2019, **9**, 1902123.
131 A. Borgschulte, R. Gremaud, S. Kato, N. P. Stadie, A. Remhof, A. Züttel, M. Matsuo and S.-I. Orimo, *Appl. Phys. Lett.*, 2010, **97**, 031916.
132 K. Kisu, S. Kim, H. Oguchi, N. Toyama and S. Orimo, *J. Power Sources*, 2019, **436**, 226821.
133 P. Ngene, P. Adelhelm, A. M. Beale, K. P. De Jong and P. E. De Jongh, *J. Phys. Chem. C*, 2010, **114**, 6163–6168.
134 S. Das, P. Ngene, P. Norby, T. Vegge, P. E. De Jongh and D. Blanchard, *J. Electrochem. Soc.*, 2016, **163**, 2029–2034.
135 F. Lu, Y. Pang, M. Zhu, F. Han, J. Yang, F. Fang, D. Sun, S. Zheng and C. Wang, *Adv. Funct. Mater.*, 2019, 1809219.
136 X. He, Y. Zhu and Y. Mo, *Nat. Commun.*, 2017, **8**, 1–7.
137 A. El kharbachi, Y. Hu, K. Yoshida, P. Vajeeston, S. Kim, M. H. Sørby, S. Orimo, H. Fjellvåg and B. C. Hauback, *Electrochim. Acta*, 2018, **278**, 332–339.
138 A. Unemoto, H. Wu, T. J. Udovic, M. Matsuo, T. Ikeshoji and S. I. Orimo, *Chem. Commun.*, 2016, **52**, 564–566.
139 W. D. Richards, L. J. Miara, Y. Wang, J. C. Kim and G. Ceder, *Chem. Mater.*, 2016, **28**, 266–273.
140 Y. Pang, X. Wang, X. Shi, F. Xu, L. Sun, J. Yang and S. Zheng, *Adv. Energy Mater.*, 2020, **10**, 1902795.
141 Y. Yan, J. B. Grinderslev, Y.-S. Lee, M. Jørgensen, Y. W. Cho, R. Černý and T. R. Jensen, *Chem. Commun.*, 2020, **56**, 3971–3974.
142 H. Liu, Z. Ren, X. Zhang, J. Hu, M. Gao, H. Pan and Y. Liu, *Chem. Mater.*, 2020, **32**, 671–678.
143 J. A. Teprovich, H. R. Colón-Mercado, P. A. Ward, B. Peters, S. Giri, J. Zhou, S. Greenway, R. N. Compton, P. Jena and R. Zidan, *J. Phys. Chem. C*, 2014, **118**, 21755–21761.
144 M. N. Guzik, R. Mohtadi and S. Sartori, *J. Mater. Res.*, 2019, **34**, 877–904.
145 L. Zhan, Y. Zhang, X. Zhuang, H. Fang, Y. Zhu, X. Guo, J. Chen, Z. Wang and L. Li, *Solid State Ionics*, 2017, **304**, 150–155.
146 Y. Zhang, L. Zhan, X. Zhuang, Y. Zhu, N. Wan, X. Guo, J. Chen, Z. Wang and L. Li, *J. Alloys Compd.*, 2017, **695**, 2894–2901.
147 A. Pradel and M. Ribes, *Solid State Ionics*, 1986, **18–19**, 351–355.
148 S. Kondo, K. Takada and Y. Yamamura, *Solid State Ionics*, 1992, **53–56**, 1183–1186.
149 K. Takada, T. Inada, A. Kajiyama, H. Sasaki, S. Kondo, M. Watanabe, M. Murayama and R. Kanno, *Solid State Ionics*, 2003, **158**, 269–274.
150 T. Inada, T. Kobayashi, N. Sonoyama, A. Yamada, S. Kondo, M. Nagao and R. Kanno, *J. Power Sources*, 2009, **194**, 1085–1088.
151 J. M. Whiteley, P. Taynton, W. Zhang and S.-H. Lee, *Adv. Mater.*, 2015, **27**, 6922–6927.
152 B. Chen, Z. Huang, X. Chen, Y. Zhao, Q. Xu, P. Long, S. Chen and X. Xu, *Electrochim. Acta*, 2016, **210**, 905–914.
153 S. Wang, X. Zhang, S. Liu, C. Xin, C. Xue, F. Richter, L. Li, L. Fan, Y. Lin, Y. Shen, J. Janek and C. W. Nan, *J. Materiomics*, 2020, **6**, 70–76.

154 J. Zheng, P. Wang, H. Liu and Y. Y. Hu, *ACS Appl. Energy Mater.*, 2019, **2**, 1452–1459.
155 L. Cong, Y. Li, W. Lu, J. Jie, Y. Liu, L. Sun and H. Xie, *J. Power Sources*, 2020, **446**, 227365.
156 A. Hayashi, T. Harayama, F. Mizuno and M. Tatsumisago, *J. Power Sources*, 2006, **163**, 289–293.
157 Z. D. Hood, H. Wang, Y. Li, A. S. Pandian, M. Parans Paranthaman and C. Liang, *Solid State Ionics*, 2015, **283**, 75–80.
158 E. Rangasamy, G. Sahu, J. K. Keum, A. J. Rondinone, N. J. Dudney and C. Liang, *J. Mater. Chem. A*, 2014, **2**, 4111–4116.
159 A. Yamauchi, A. Sakuda, A. Hayashi and M. Tatsumisago, *J. Power Sources*, 2013, **244**, 707–710.
160 B. Kubíková, J. Mlynáriková, O. Beneš, E. Mikšíková, J. Priščák, A. Tosolin and M. Boča, *J. Mol. Liq.*, 2018, **268**, 754–761.
161 N. Garg, A. K. Mishra, H. K. Poswal, A. K. Tyagi and S. M. Sharma, *J. Solid State Chem.*, 2015, **229**, 164–172.
162 S. Muy, J. Voss, R. Schlem, R. Koerver, S. J. Sedlmaier, F. Maglia, P. Lamp, W. G. Zeier and Y. Shao-Horn, *iScience*, 2019, **16**, 270–282.
163 R. Schlem, S. Muy, N. Prinz, A. Banik, Y. Shao-Horn, M. Zobel and W. G. Zeier, *Adv. Energy Mater.*, 2020, **10**, 1903719.
164 X. Li, J. Liang, N. Chen, J. Luo, K. R. Adair, C. Wang, M. N. Banis, T. Sham, L. Zhang, S. Zhao, S. Lu, H. Huang, R. Li and X. Sun, *Angew. Chem.*, 2019, **131**, 16579–16584.
165 K. H. Park, K. Kaup, A. Assoud, Q. Zhang, X. Wu and L. F. Nazar, *ACS Energy Lett.*, 2020, **5**, 533–539.
166 K. Yamada, K. Kumano and T. Okuda, *Solid State Ionics*, 2006, **177**, 1691–1695.
167 S. Wang, Q. Bai, A. M. Nolan, Y. Liu, S. Gong, Q. Sun and Y. Mo, *Angew. Chem., Int. Ed.*, 2019, **58**, 8039–8043.
168 J. Liang, X. Li, S. Wang, K. R. Adair, W. Li, Y. Zhao, C. Wang, Y. Hu, L. Zhang, S. Zhao, S. Lu, H. Huang, R. Li, Y. Mo and X. Sun, *J. Am. Chem. Soc.*, 2020, **142**, 7012–7022.
169 A. R. Polu, D. K. Kim and H. W. Rhee, *Ionics*, 2015, **21**, 2771–2780.
170 A. R. Polu and H. W. Rhee, *Int. J. Hydrogen Energy*, 2017, **42**, 7212–7219.
171 E. Quartarone and P. Mustarelli, *Chem. Soc. Rev.*, 2011, **40**, 2525–2540.
172 Y.-S. Hu, *Nat. Energy*, 2016, **1**, 1–2.
173 Z. Zou, Y. Li, Z. Lu, D. Wang, Y. Cui, B. Guo, Y. Li, X. Liang, J. Feng, H. Li, C. W. Nan, M. Armand, L. Chen, K. Xu and S. Shi, *Chem. Rev.*, 2020, **120**, 4169–4221.
174 X. Li, J. Liang, X. Yang, K. R. Adair, C. Wang, F. Zhao and X. Sun, *Energy Environ. Sci.*, 2020, **13**, 1429–1461.
175 J. Zheng, M. Tang and Y.-Y. Hu, *Angew. Chem., Int. Ed.*, 2016, **55**, 12538–12542.
176 L. Yang, Z. Wang, Y. Feng, R. Tan, Y. Zuo, R. Gao, Y. Zhao, L. Han, Z. Wang and F. Pan, *Adv. Energy Mater.*, 2017, **7**, 1–9.
177 C. Monroe and J. Newman, *J. Electrochem. Soc.*, 2004, **151**, A880–A886.
178 Z. Ahmad and V. Viswanathan, *Phys. Rev. Lett.*, 2017, **119**, 056003.
179 C. Monroe and J. Newman, *J. Electrochem. Soc.*, 2003, **150**, A1377–A1384.
180 P. Albertus, S. Babinec, S. Litzelman and A. Newman, *Nat. Energy*, 2018, **3**, 16–21.
181 C. Fu, V. Venturi, J. Kim, Z. Ahmad, A. W. Ells, V. Viswanathan and B. A. Helms, *Nat. Mater.*, 2020, **19**, 758–766.
182 M. B. Dixit, M. Regala, F. Shen, X. Xiao and K. B. Hatzell, *ACS Appl. Mater. Interfaces*, 2019, **11**, 2022–2030.
183 F. Shen, M. B. Dixit, X. Xiao and K. B. Hatzell, *ACS Energy Lett.*, 2018, **3**, 1056–1061.
184 M. J. Zachman, Z. Tu, S. Choudhury, L. A. Archer and L. F. Kourkoutis, *Nature*, 2018, **560**, 345–349.
185 J. Zheng and Y. Y. Hu, *ACS Appl. Mater. Interfaces*, 2018, **10**, 4113–4120.
186 M. B. Dixit, W. Zaman, N. Hortance, S. Vujic, B. Harkey, F. Shen, W. Y. Tsai, V. De Andrade, X. C. Chen, N. Balke and K. B. Hatzell, *Joule*, 2020, **4**, 207–221.
187 R. Chen, Q. Li, X. Yu, L. Chen and H. Li, *Chem. Rev.*, 2020, **120**(14), 6820–6877.
188 R. Chen, A. M. Nolan, J. Lu, J. Wang, X. Yu, Y. Mo, L. Chen, X. Huang and H. Li, *Joule*, 2020, **4**, 812–821.
189 Z. Fan, B. Ding, T. Zhang, Q. Lin, V. Malgras, J. Wang, H. Dou, X. Zhang and Y. Yamauchi, *Small*, 2019, **15**, 1903952.